Ultrasonics

Generalised Bisection Method for Optimum Ultrasonic Ray Tracing and Focusing in Multi-Layered Structures

--Manuscript Draft--

Manuscript Number:	ULTRAS-D-20-00550R1
Article Type:	Research Paper
Section/Category:	Physical aspects of wave propagation
Keywords:	Ultrasonic wave propagation; Ray tracing; Mathematical modelling; Bisection method; Multi-layered structures; Weld inspection; Composites
Corresponding Author:	Carmelo Mineo, Ph.D Universita degli Studi di Palermo Palermo, Italy ITALY
First Author:	Carmelo Mineo, Ph.D
Order of Authors:	Carmelo Mineo, Ph.D
	David Lines
	Donatella Cerniglia, Ph.D
Abstract:	Ultrasonic testing has been used for many decades, proving itself very efficient for detecting defects in many industrial sectors. The desire to apply ultrasonic testing to geometrically complex structures, and to anisotropic, inhomogeneous materials, together with the advent of more powerful electronics and software, is constantly pushing the applicability of ultrasonic waves to their limits. General ray tracing models, suitable for calculating the proper incident angle of single element probes and the proper time delay of phased array, are currently required. They can support the development of new imaging techniques, as Full Matrix Capture and Total Focusing Method, and the execution of very challenging ultrasonic inspections. This paper introduces a generalized iterative method for the computation of ultrasonic ray paths, when ultrasonic source and target are separated by multiple complex material interfaces in the two dimensional and three dimensional domains. The manuscript starts with a review of the well-known bisection method, and extends the applicability of the method to cases with increasing complexity. An application example, in the field of in-process weld inspection, shows that the introduced generalised bisection method can enable the computation of optimum incidence angles and focal delays for accurate ultrasonic focusing. There is no restriction on the analytical interfaces to be surjective. Interface folding is permitted. It is not necessary to know, a priori, with what sequence the interfaces are crossed by the rays. The presented implementation of the method completes each iteration of the bisection method in 4ms, for a case with a single interface, and in 960ms for the case with 52 interfaces.
Suggested Reviewers:	Bruce Drinkwater, Ph.D Professor, University of Bristol b.drinkwater@bristol.ac.uk Prof. Drinkwater leads a research group working on ultrasonics and non-destructive testing. His research interests span pretty much anything with any connection to ultrasonics. He has published more than 100 journal articles. Most of his publications concern ultrasonic wave propagation and industrial applications.
	Paul Wilcox, Ph.D Professor, University of Bristol p.wilcox@bristol.ac.uk Professor Wilcox is a renowned expert in elastodynamic wave propagation and scattering, Ultrasonic arrays, Signal processing, Structural Health Monitoring and Non-Destructive Testing
	Anthony Mulholland, Ph.D Professor, University of Bristol anthony.mulholland@bristol.ac.uk Professor Mulholland is a mathematician, expert in modelling problems in engineering,

	chemistry, biology, mathematics and statistics, physics, material science and computing. His publications show he has a great interest in Non-Destructive Evaluation through ultrasonic methods.
Response to Reviewers:	We thank the reviewers for the time and efforts they put in reviewing our work and in producing clear and useful comments. We believe this revision improves the quality of the article. Therefore, we are pleased to submit the revised manuscript, where all changes have been highlighted using the “Track Changes” tool of Microsoft Word. Our answers to each one of the reviewers’ comments are also clearly listed in a separate document.

Dr Carmelo Mineo
Marie-Curie Research Fellow
Department of Engineering
University of Palermo
Viale delle Scienze, Edificio 8
90128 Palermo, Italy
carmelo.mineo01@unipa.it

21st October 2020

Dear Editor-in-Chief,

I and my co-authors are glad to submit the revised version of our manuscript entitled "*Generalised Bisection Method for Optimum Ultrasonic Ray Tracing and Focusing in Multi-Layered Structures*".

We thank the reviewers for the time and efforts they put in reviewing our work and in producing clear and useful comments. We addressed all flagged issues. We believe this revision improves the quality of the article. We are pleased to submit the revised manuscript, where all changes have been highlighted through using the "Track Changes" tool of Microsoft Word. Our answers to each one of the reviewers' comments are also provided and clearly listed in a separate document we prepared.

This work is original, it has not been published elsewhere and it is not under consideration for publication elsewhere.

The paper introduces a generalized iterative method for the computation of ultrasonic ray paths, when ultrasonic source and target are separated by multiple complex material interfaces in the two and three dimensional domain. The manuscript starts with a review of the well-known bisection method, and extends the applicability of the method to cases with increasing complexity. We present the detailed mathematical formulation of the method to help the scientific community to take advantage of the implementation of the method in ongoing research and in industrial applications. We have chosen to include an interesting application example, concerning the field of in-process weld inspection. This example shows how the introduced generalised bisection method enables the computation of optimum incidence angles and focal delays for accurate ultrasonic focusing in complex scenarios. Qualitative and quantitative performance results are presented.

The paper is aligned with the key topics covered by the journal. In particular, this is a high-quality, original research paper with scientific merit and novelty, introducing significant advancements in the comprehension of the ultrasonic wave propagation in multi-layer three dimensional structures. This can have an immediate application to the fields of ultrasonic NDT/SHM and their industrial applications.

I am a Research Fellow of the University of Palermo (Italy), affiliated to the Department of Engineering. My co-authors and I have already successfully published the outcomes of our research in excellent peer-reviewed journals, comprising *Ultrasonics*, in the past. Your journal is the best place to publish this new work.

Thank you for considering our manuscript. Do not hesitate to let we know if a further revision is required by the reviewers.

Yours Sincerely,

Carmelo Mineo

Manuscript Number: ULTRAS-D-20-00550

Generalised Bisection Method for Optimum Ultrasonic Ray Tracing and Focusing in Multi-Layered Structures

Authors' answers to reviewers' comments

Each one of the reviewers' comments is reported in bold and is followed by a bullet point with the authors' answer. All changes applied to the manuscript have been highlighted through the "Track Changes" tool of Microsoft Word.

Reviewer #1:

Comments

1. **A very nice paper which has developed an ultrasonic wave ray tracing method based on refraction (Snell's Law) where the wave is passing through a series of isotropic layers.**
    - We thank the reviewer for the time and efforts put in the review of our work.

2. **The method has been generalised to the three dimensional case. These layers can have curved interfaces provided that there is a one-to-one map from the x-y plane to each interface. In other words the layers can be described by z=f(x,y) and so folding is not permitted. The use of this method is to inform the delay laws in an ultrasonic transducer array to enable it to focus on a specific point in the layered domain. The method therefore requires knowledge of the wave velocity in each layer, the functions describing the shape of each layer to layer interface, and the particular spatial point to be focused upon. The method was successfully tested on some simulated data sets in the latter part of the paper.**
    - Note, the current implementation is able to support any kind of interfaces. There is no restriction on the analytical interfaces to be defined in the x-y domain. The interfaces can tilt and folding is permitted. For every refraction, the analytic equation of the line for the last intersection point, whose direction is given by the unitary refraction vector, is intersected in turn with all the analytic functions of the interfaces. This operation gives one intersection point for each interface surface. The interface that produces the closest point to the last intersection point is selected as the correct intersection surface and the point is returned as the location where a new refraction takes place. This continues until the horizontal plane for the target (T) is reached. For this reason, which maximises the usefulness of the proposed implementation, there is a quadratic dependence between the computation time and the number of interfaces (see Table 2). The dependence would be linear if the sequence of intersected surfaces is defined, but the method would only be applicable to layered material.

3. **I would suggest using the phrases "two dimensional" and "three dimensional" throughout the manuscript rather than "bi-dimensional" and "tri-dimensional" which are non-standard.**
    - All instances of "bi-dimensional" and "tri-dimensional" have been replaced with "two dimensional" and "three dimensional".

4. **In Section 2 you describe the Bisection Method. Can you explain why this method was chosen over other root finding algorithms? The bisection method is well known to be slow to converge when compared to Newton type methods for example.**

    - The reviewer is right. The bisection method is well known to be slow to converge when compared to Newton type methods. If we are interested in the solution of $f(x) = 0$ and we have access to the derivative of $f(x)$ as well as a good rough estimate of the root, then the Newton type methods would give us a quadratic convergence (at least two extra digits of the root per iteration). However, the increased speed of convergence comes with more ways to fail. The method is sensitive to the choice of the initial condition and the smoothness of $f(x)$. Iterations can overshoot the root, or get locked into a periodic iteration forever. If the initial condition is also a critical point, i.e., $f'(x^*) = 0$, or close to a critical point, the method cannot even start. In fact, multiplicity of a root can slow down the method. Getting a good initial estimate for x^* is tricky, especially in high-dimensional examples. The bisection method needs an interval (or whatever its generalization in higher dimensions) that contains the root and $f(x)$ has to be a continuous function. With those assumptions, convergence is guaranteed and it is linear with respect to the iterations. So, in terms of convergence speed, Newton's methods outperform the bisection method. However, they need information about the derivative or about the partial derivatives (for multi-dimensional functions). In terms of information about $f(x)$, the bisection method requires much less. Thus, this is the reason why the bisection method was chosen over other root finding algorithms, for this work. Nevertheless, the authors envisage future work focusing on the application of faster root finding algorithms. The authors' aim is to investigate the efficiency of a combination of bisection and Newton's methods in ultrasonic ray tracing, where the bisection approach would be used until a rough estimate of the root is found and the Newton's method would be used to refine the estimate.

5. **Page 4, Equation(6). Please note that there is an identity tan(asin(x))=x/Sqrt[1-x^2]. Use of such an identity may well speed up your algorithm. You may wish to comment in the paper.**

    - We thank the reviewer for helping us to refine the math. This has been included in the paper through a revised version of Equation 6 and the accompanying text.

6. **Page 9, Line -5. When you say "horizontal plane" do you mean the plane that passes through P1 and has normal vector k=(0,0,1)^T ? So that is the plane z=f1(p1)? If so then please state this.**

    - The reviewer is right. This comment and the following comment have been addressed by replacing the original paragraph, which introduced the planes ω_1 and τ_1, with the following text: *"The plane ω_1 is the horizontal plane that passes through P_1 and has normal vector $[0 \quad 0 \quad 1]^T$, which is the plane described by the equation: $z = f_1(P_1)$. The plane τ_1 is the plane tangent to the surface $f_1(x, y, z) = 0$ in P_1, whose normal coincides with $\vec{n}_1$."*

7. **Page 9, Line -5. Does the plane tau_1 have normal vector n_1 ? If so then state this.**

    - The reviewer is right. This comment has been addressed, as per answer to the previous comment.

8. **Page 9. Equation (20). The notation in equation (20) has "n_1" and yet you have used the notation "n_{P1}" in equation (21). Please use one of these for consistency.**

- Thank you to the reviewer for spotting this inconsistency. This has been fixed.

9. **Same comment as 6. For equation (23).**
    - Fixed, as per comment 6.
10. **p19, line -10: State how many iterations the method took typically to converge.**
    - The average number of iterations has been included in Table 2, as additional quantitative performance parameter. The typical number of iterations is slightly bigger than 13 and does not seem to be influenced by the number of interface surfaces in the model.
11. **p20, line 4: You mention that your method is much faster than a FEM code. What about using the Fast-Marching Method (FMM) (i.e. solving the Eikonal equation) combined with Fermat's Principle to do the ray tracing. How would your method compare with that approach? The FMM does not care if the medium is layered or indeed just a partition of regions with differing material properties such as a weld region. Indeed, you can implement Fermat's principle by viewing the domain as a grid of connected points and then use Dijkstra's algorithm. At the very least you should mention this an alternative approach in the literature review section and in the conclusions as an alternative method. You could cite Nowers, O, Duxbury, DJ, Zhang, J & Drinkwater, BW, 2014, 'Novel ray-tracing algorithms in NDE: Application of Dijkstra and A* algorithms to the inspection of an anisotropic weld'. NDT and E International, vol 61., pp. 58-66 10.**
    - We thank the reviewer for this interesting comment. The proposed generalization of Snell's law to the three-dimensional case is not limited to layered medium. It is applicable to situations where there are partitions, as long as the interface of the partitions are described by analytical equations. Each iteration of the bisection method advances looking for the interface surface that is intersected by the ray. We have inserted a note related to the use of Dijkstra's algorithm in the introduction. The recommended paper has also been cited in the introduction and in the conclusion as an alternative method.
12. **p20, line -3: You mention "anisotropic" media. How would you extend your method to a layered medium where each layer was anisotropic? In such a case you would need to take into account the orientation of the tensor describing the anisotropic material (eg the slowness surface) AND the angle that the ray enters that region. Please note that the FMM has been extended to heterogeneous materials where each region (for example layer but again can be a partitioning into a random collection of locally anistropic regions such as a weld) is anisotropic. You could cite in the introduction/conclusion K. M. M. Tant, E. Galetti, A. J. Mulholland, A. Curtis & A. Gachagan (2020) Effective grain orientation mapping of complex and locally anisotropic media for improved imaging in ultrasonic non-destructive testing, Inverse Problems in Science and Engineering, DOI: 10.1080/17415977.2020.1762596**
    - Our claim is motivated by the fact that the proposed method allows computing the angle that the ray enters each region. So, it enables considering the anisotropy of the medium through the tensor describing the anisotropic material in every region. Obviously, this would require building onto the presented generalized algorithm. The scope of the paper is limited to presenting the mathematical formulation required to generalize Snell's

law to the three-dimensional case. As it was suggested, the recommended work has been cited in the introduction of the manuscript.

Typographical Errors

13. **In various places you have used the phrase "bisecting method" and it should be "bisection method".**
    - All occurrences of "bisecting method" have been replaced with "bisection method".
14. **In p9, equation (20) (and the line above) you have used the Greek letter uppercase delta to denote Grad. You should use the standard notation of nabla. Which is an inverted delta.**
    - Thanks to the reviewer for spotting this mistake. The issue has been fixed.
15. **p9, 2 lines after equation (20). Replace "lays on" with "lies in"**
    - Done
16. **p10, line -9. Remove "the" to read "imposition of Snell's law…."**
    - Done
17. **p13, line 3. Add "s" to "function".**
    - Done
18. **p14, line 1: replace "such" with "the"**
    - Done
19. **p14, line 7: "finale" should be "final"**
    - Done
20. **p15, line 1: should read "inspection of"**
    - Done
21. **p16, line 5: add "the" before "sake"**
    - Done
22. **p19, line -3: spelling "discrete"**
    - Done

Reviewer #2:

Comments

1. **This paper has a number of issues which preclude publication in its current format.**
    - Thanks to the reviewer for the time and efforts put into the review of our work. The reviewer's comments are answered below. We believe our corrections address the comments and improve the quality of the manuscript.

2. **The abstract reads like a shortened introduction, with no mention of their (limited) findings.**

- We thank the reviewer for this criticism. The abstract has been revised. Mention of other existing methods, features of the proposed approach and results have been added.

3. **In the introduction, no detail of current ray tracing methods is presented, as we only have a single sentence to work with: "To increase imaging speed, and improve focusing and/or steering of phased array (PA) ultrasonic beams on the desired position, several works have investigated ways to compute the ultrasonic ray paths [9-11]." What alternatives are available to the bisection method introduced in section 2? How does this approach provide benefits over other methods? This cuts to one of the criticisms of this paper - it provides a method which it compares (time-wise) to finite element simulation. However, ray-based modelling is common, so their method should be compared against ray-based alternatives.**

    - The scope of the paper is focused to presenting the mathematical formulation required to generalize Snell's law to the three-dimensional case. We believe this can find applicability to several scenarios. Nevertheless, we thank the reviewer for inviting us to refine the review of the state of the art. We have inserted a note related to an alternative method based on the use of Fast-Marching Method (FMM), combined with Fermat's Principle, to do the ray tracing. It has also been highlighted that the FMM has been extended to heterogeneous materials. The following two works have been included in the references:

        i. Nowers, O, Duxbury, DJ, Zhang, J & Drinkwater, BW, 2014, 'Novel ray-tracing algorithms in NDE: Application of Dijkstra and A* algorithms to the inspection of an anisotropic weld'. NDT and E International, vol 61., pp. 58-66 10.

        ii. K. M. M. Tant, E. Galetti, A. J. Mulholland, A. Curtis & A. Gachagan (2020) Effective grain orientation mapping of complex and locally anisotropic media for improved imaging in ultrasonic non-destructive testing, Inverse Problems in Science and Engineering, DOI: 10.1080/17415977.2020.1762596

4. **The authors have followed a sensible approach by increasing the model complexity as it moves from 2d flat to curved surfaces and finally 3d curved. However, presentation of the equations used for these scenarios is questionable. An appendix should definitely be considered. For example, equation 34 is actually an if-elseif statement covering 2/3rd of a page. The same is true of equation 35.**

    - Thanks to the reviewer for the suggestion. Equation 34 and 35 have been moved respectively to Appendix A and Appendix B, after the references. The numbering of the other equations has been adjusted accordingly.

5. **The authors undermine their complexity staircase by only considering one demonstration example in the results. Although initially presented in 3d, it is just a 2d problem with flat interfaces - as is neatly summarised in figure 7. Figure 7 also highlights the necessary editing required of this paper. It contains 3 parts, but only Figure 7(c) is necessary! This is also true in other figures, such as Figure 8 (remove (a) and move numbering to (b)).**

    - The authors thought carefully about a suitable example to describe the use of the mathematical formulation presented in this work. Eventually, the in-process butt-welded plate was selected as a good example. The reviewer is right in observing that, although the paper presents the generalization of Snell's laws to the three-dimensional case, a two-dimensional formulation

would be sufficient for the proposed example. Indeed, by neglecting the evolution of the temperature in the y-direction of the welded model, the problem is reduced to a 2D case. This approach was pursued by the authors just to make the example and all figures more easily comprehensible by the readers. Following the reviewer's comment Figure 7b is removed and Figure 7c is renamed as Figure 7b. The authors deemed useful to keep Figure 7a since it helps visualize the eleven temperature zones across the specimen, with relative sound speed in the material. Likewise, the authors have decided to not remove Figure 8a. Moving the numbering of the interface surfaces from Figure 8a to Figure 8b would make Figure 8b too confusing. Whereas Figure 8a gives the numbering of all surfaces, Figure 8b is dedicated to highlighting the interfaces intersected by the ultrasonic rays. Hopefully, this can be deemed acceptable by the reviewers and editor too.

6. **In section 6, the authors propose that their method is suitable for real-time in-process welding inspection. This would suggest a rapid calculation would be required, something that the results presented in the paper certainly do not suggest is currently possible.**

    - We highlight that the implementation of the proposed method was not optimized for speed. Although the current result is already a great advantage if compared to the time required by Finite Element models, more work is required to produce more sophisticated implementations of the method, capable of minimizing the execution time without compromising the accuracy. This is also mentioned as future work in the conclusions. In terms of convergence speed, Newton's methods outperform the bisection method. However, they need information about the derivative or about the partial derivatives. The bisection method requires much less. Thus, this is the reason why the bisection method was chosen over other root finding algorithms, for this work. However, we envisage future work focusing on the application of faster root finding algorithms. The authors' aim is to investigate the efficiency of a combination of bisection and Newton's methods in ultrasonic ray tracing, where the bisection approach would be used until a rough estimate of the root is found and the Newton's method would be used to refine the estimate. Nevertheless, taking advantage of this revision, some improvements have been added to the presented implementation, reducing the computation time of each iteration of the bisection method to 3.98 ms, for the case with a single interface, and to 960.36 ms, for the case with 52 interfaces. The convergence time for each ray depends on the stopping criteria, which affects the number of required iterations. Moreover, the proposed algorithms can be used to pre-calculate a number of focal laws for the geometry (e.g. with differing temperature profiles). During the inspection, the temperature sensors are used to select the most appropriate match for the thermal profile.

7. **They present an anisotropic problem, due to temperature gradient, as one capable of being determined using a piecewise isotropic approach. When comparing either 27 and 52 interfaces, they conclude that "This seems to suggest that the dependence between the computation time of the current method and the number of surfaces in the model could be described by a linear or a subquadratic law". Why is this conclusion drawn from only 2 data points?**

    - We had used three points (1, 27 and 52 interfaces) to infer the dependence of the computation time from the number of interfaces. Nevertheless, we accept the reviewer's criticism and acknowledge that more points should have been used. Four more points were added (7, 17, 37 and 47 interfaces),

for a total of 7 points (1, 7, 17, 27, 37, 47 and 52 interfaces). The corresponding computation times are given in Table 2. Beside the total elapsed time, the revised version of Table 2 also contains the average number of iterations, the average duration of each iteration and the average convergence time for each ray. The average duration of each iteration is the best parameter to investigate the dependence between the computation time and the number of interfaces, since such parameter is independent from the stopping criteria, which influence the number of iterations of the bisecting method, and the number of sources (elements) in the ultrasonic phased array probe. This confirmed a quadratic relationship between the computation time and the number of interfaces, as it is illustrated in the picture below.

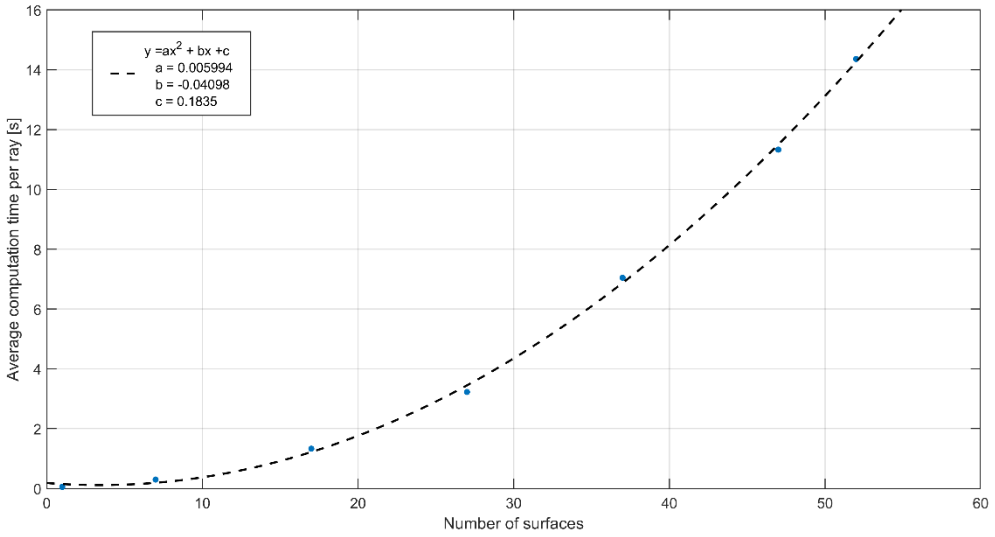

Note, the current implementation is able to support any kind of interfaces. There is no restriction on the analytical interfaces to be defined in the x-y domain. The interfaces can tilt and fold. For every refraction, the analytic equation of the line for the last intersection point, whose direction is given by the unitary refraction vector, is intersected in turn with all the analytic functions of the interfaces. This operation gives one intersection point for each interface surface. The interface that produces the closest point to the last intersection point is selected as the correct intersection surface and the point is returned as the location where a new refraction takes place. This continues until the horizontal plane for the target (T) is reached. This is the reason of the quadratic dependence between the computation time and the number of interfaces. This aspect, which was already highlighted in the section 6, has been mentioned in the abstract too. The dependence would be linear if the sequence of intersected surfaces is defined (e.g. the case of a layered composite material).

8. **The best times provided by the method are approximately 42 seconds when modelling an isotropic plate medium (only 1 interface, the wedge/plate). This seems high for calculating only 64 rays (64 start points, 1 end point and 1 interface), even for a MATLAB implementation. When considering the best piecewise isotropic approach with 52 interfaces, this time increases to 21 minutes. How do other ray approaches perform?**

    - As is was said in the answer to comment n.5, some improvements have been added to the presented implementation, taking advantage of this revision. We achieved to reduce the computation time of each iteration of

the bisection method has been reduced to from 42 to 3.4 seconds, when modelling an isotropic plate medium (only 1 interface, the wedge/plate), and from 21 to 15 minutes, for the case with 52 interfaces. As it was explained in the answer to the previous comment, there is a quadratic dependence between the computation time and the number of interfaces. The dependence would be linear if the sequence of intersected surfaces is defined (e.g. the case of a layered composite material).

With this being said, the scope of this work is focused to presenting the mathematical formulation required to generalize Snell's law to the three-dimensional case. We believe it can find applicability to several scenarios. However, since the implementation of the method was not optimized for speed, we did not compare it to the performance of other method. Indeed, we aim to focus the future work on generating more sophisticated implementations of the method, capable of minimizing the execution time without compromising the accuracy.

9. **Why is an accuracy of 0.01mm required? What effect does this required accuracy negate?**

    - One or more stopping criteria are required in iterative convergence methods. Obtaining a distance from target smaller than 0.01mm has been used as stopping criteria in our work. There is nothing this negate. The stopping criteria can be different, depending on the application. In practical applications of the method, a meaningful approach would be to stop iterating when the change in transit time is smaller than a defined fraction of a wavelength. A note about this has been added to the manuscript (page 17).

10. **Only relative metrics are presented, e.g. mean shift in transit time. For ease of future validation, absolute metrics should be provided, with relative ones an optional extra.**

    - The reviewer is right about this. We apologise for not having payed attention to this before. The relative metrics (distance from target and shift in travel time) have been moved from Table 2 to a new table (Table 3). Also, the requested absolute metrics (travel distance and travel time) have been included in Table 3, for all cases. The text of section 6 has been edited to introduce the new table and the new reported data.

11. **In summary, the method the authors introduce should be considered "not proven". The single example given doesn't cover the majority of the theory, with sections 4 and 5 unused. Also, the results are not validated against any other method.**

    - This comment is answered by the answer to comment n.5.

Highlights

- The work introduces a generalized iterative method for computation of ultrasonic ray paths;
- Ray tracing through multiple complex interfaces in the two and three dimensional domains;
- Enabling the computation of optimum incidence angles for accurate ultrasonic focusing;
- Application example in the field of in-process weld inspection.

Generalised Bisection Method for Optimum Ultrasonic Ray Tracing and Focusing in Multi-Layered Structures

Carmelo Mineo*[1], David Lines[2], Donatella Cerniglia[1]

*Corresponding author (carmelo.mineo01@unipa.it)

1 - Department of Engineering, University of Palermo, Viale delle Scienze, Edificio 8, 90128 Palermo, Italy.

2 - Department of Electronic & Electrical Engineering (EEE), University of Strathclyde, 204 George St, Glasgow G1 1XW, UK.

ABSTRACT

Ultrasonic testing has been used for many decades, proving itself very efficient for detecting defects in many industrial sectors. ~~Due to it being inexpensive and much safer than other non-destructive testing techniques, ultrasonic testing remains a hot research topic, since researchers try to extend and maximize its applicability to challenging parts and new industrial areas.~~ The desire to apply ultrasonic testing to geometrically complex structures, and to anisotropic, inhomogeneous materials, together with the advent of more powerful electronics and software, is constantly pushing the applicability of ultrasonic waves to their limits. General ray tracing models, suitable for calculating the proper incident angle of single element probes and the proper time delay of phased array, are currently required. They can support the development of new imaging techniques, as Full Matrix Capture and Total Focusing Method, and the execution of very challenging ultrasonic inspections. This paper introduces a generalized iterative method for the computation of ultrasonic ray paths, when ultrasonic source and target are separated by multiple complex material interfaces in the ~~bi-~~ two dimensional and ~~tri-dimensional~~ three dimensional domains. The manuscript starts with a review of the well-known bisection method, and extends the applicability of the method to cases with increasing complexity. An application example, in the field of in-process weld inspection, shows that the introduced generalised bisection method can enable the computation of optimum incidence angles and focal delays for accurate ultrasonic focusing. There is no restriction on the analytical interfaces to be surjective. Interface folding is permitted. It is not necessary to know, a priori, with what sequence the interfaces are crossed by the rays. The presented implementation of the method completes each iteration of the bisection method in 4ms, for a case with a single interface, and in 960ms for the case with 52 interfaces.

Keywords: Ultrasonic wave propagation, Ray tracing, Mathematical modelling, Bisection method, Multi-layered structures, Weld inspection, Composites.

1. INTRODUCTION

Ultrasonic testing (UT) is a family of non-destructive testing techniques based on the propagation of ultrasonic waves in the object or material tested. In most common UT applications, very short ultrasonic pulse-waves with centre frequencies ranging from 0.1-15 MHz, and occasionally up to 50 MHz, are transmitted into materials to detect internal flaws or to characterize materials. Ultrasonic testing is often performed on steel, concrete, wood and composites. It is used in many industries including steel and aluminium construction, metallurgy, manufacturing, petrochemical, aerospace, automotive and other transportation sectors [1, 2]. UT inspection of

planar components is relatively straightforward. However, the inspection of components with nonplanar surface geometries, such as weld-caps, curved pipes, and curved composite structures is more challenging and requires specific technologic solutions. Various works have addressed the inspection of curved components and developed ways to couple the ultrasonic transducers with the material under test, using flexible ultrasonic arrays conforming to the surface [3], deploying a rigid array on a nearby planar surface to image the region of interest from the side either directly [4] or by using signals reflected from the back wall of the component [5]. Another option is to use an intermediary layer (e.g., a solid shoe with a surface conformal with that of the component or water), to couple the transducer to the component [6-8]. However, the imaging speed depends on the complexity of the surface and the total number of image pixels, and this is a key concern for industrial end-users. To increase imaging speed, and improve focusing and/or steering of phased array (PA) ultrasonic beams on the desired position, several works have investigated ways to compute the ultrasonic ray paths [9-11]. One solution is to use the Fast-Marching Method (FMM) combined with Fermat's principle, considering the domain of interest as a grid of connected points, and then use Dijkstra's algorithm [12]. FMM has been extended to heterogeneous materials, where each region can be anisotropic [13]. ~~Despite these efforts~~However, a general ray tracing model based on Snell's law, suitable for calculating the proper incident angle of single element probes and the proper time delay of phased array probes in ~~bi-dimensional~~ two and ~~tri-dimensional~~ three dimensional multi-layer parts, and in anisotropic and inhomogeneous materials, is still missing. This paper introduces a generalized iterative method for the computation of ultrasonic ray paths, when ultrasonic source and target are separated by multiple complex material interfaces in the ~~bi-~~ two and ~~tri-dimensional~~ three dimensional domains. The manuscript starts with a review of the well-known bisection method in Section 2. It then demonstrates the application of the method to cases with increasing complexity (flat material interfaces in Section 3 and curved ~~bi-dimensional~~ two dimensional interfaces in Section 4), concluding with the generalisation of the method for its applicability to ray tracing through multiple complex interfaces in the ~~tri-dimensional~~ three dimensional domain. The paper discusses application examples and results in Section 6 and draws the conclusions in Section 7.

2. BISECTION METHOD

The bisection method is a root-finding method that applies to any continuous functions for which one knows two values with opposite signs [14]. The method consists of repeatedly bisecting the interval defined by these values and then selecting the subinterval in which the function changes sign, and therefore must contain a root. The method is also called the interval halving method [15], the binary search method [14], or the dichotomy method [16].

The method is applicable for numerically solving the equation $f(x) = 0$ for the real variable x, where $f(x)$ is a continuous function defined on an interval $[a, b]$ and where $f(a)$ and $f(b)$ have opposite signs. In this case a and b are said to bracket a root since, by the intermediate value theorem, the continuous function $f(x)$ must have at least one root in the interval (a, b). The interval halving method is an iterative method. At each iteration the method divides the interval in two by computing the midpoint $c = \frac{(a+b)}{2}$ of the interval and the value of the function $f(c)$. Unless c is itself a root (which is very unlikely, but possible), there are only two possibilities: either $f(a)$ and $f(c)$ have opposite signs and bracket a root, or $f(c)$ and $f(b)$ have opposite signs and bracket a root. The method selects the subinterval that is guaranteed to be a bracket as the new interval to be used in the

next iteration. Explicitly, if $f(a)$ and $f(c)$ have opposite signs, then the method sets c as the new value for b, and if $f(c)$ and $f(b)$ have opposite signs then the method sets c as the new a. In both cases, the new $f(a)$ and $f(b)$ have opposite signs, so the method is applicable to this smaller interval. In this way, the interval that contains a zero of $f(x)$ is reduced in width by 50% at each iteration. The process is continued until the interval is sufficiently small or if $f(c) = 0$. Then c is taken as the root of the function and the process stops.

3. FLAT MATERIAL INTERFACES

Given a source of ultrasonic energy in a point S and defining the point T as the target point, where one wants to send the energy, Figure 1 shows the ultrasonic ray tracing for multiple material layers, in the ~~bi-dimensional~~ two dimensional case. Although the figure illustrates the ray tracing for the case of a structure with four material layers, the algorithms presented in this work are generalized for k layers, with k being not predetermined.

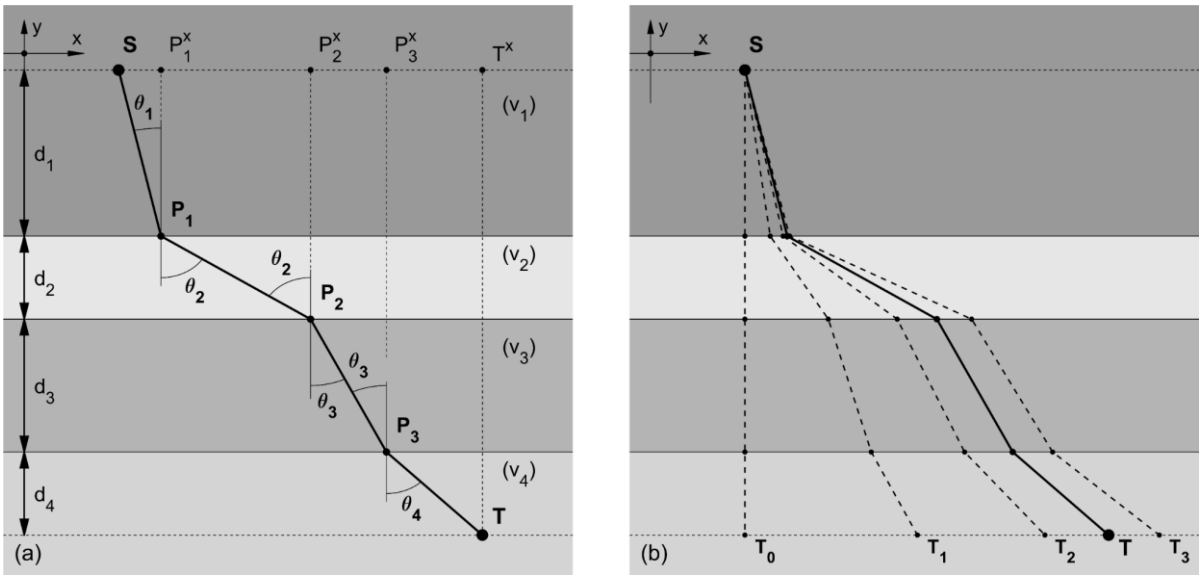

Figure 1 – (a) Annotated ultrasonic ray tracing for multiple material layers in the ~~bi-dimensional~~ two dimensional case and (b) convergence to solution through the ~~bisecting method~~ bisection method.

Thus, using the notation in Figure 1a and generalizing for k layers, the following equation is valid:

$$\overline{SP_1^x} + \left(\sum_{i=2}^{k-1} \overline{P_{i-1}^x P_i^x}\right) + \overline{P_{k-1}^x T^x} = \overline{ST^x} \tag{1}$$

Considering that the lengths of the segments on the left-hand side of the equation are equal to the product of the layer thicknesses (d_i) and the tangents of the angles of incidence/refraction (θ_i), in each layer, we have:

$$d_1 \cdot \tan\theta_1 + \left(\sum_{i=2}^{k-1} d_i \cdot \tan\theta_i\right) + d_k \cdot \tan\theta_k = \overline{ST^x} \tag{2}$$

$$d_1 \cdot \tan\theta_1 + \left(\sum_{i=2}^{k} d_i \cdot \tan\theta_i\right) = \overline{ST^x} \tag{3}$$

The relationship between the angles of incidence and refraction, when referring to waves passing through a boundary between two different isotropic media, is described by the Snell's law (also known as Snell-Descartes law and the law of refraction) [17]. The law follows from Fermat's principle of least time [18]. Snell's law states that the ratio of the sines of the angles of incidence and the speed of propagation of the wave is equivalent to the

ratio of the sine of the refracted angle and the propagation speed in the media where the wave is refracted. Therefore, the following is valid:

$$\frac{\sin\theta_1}{v_1} = \cdots = \frac{\sin\theta_i}{v_i} = \cdots = \frac{\sin\theta_k}{v_k} \tag{4}$$

Note that each angle is measured from the normal of the boundary interface and the propagation velocities in the respective media are inserted in the formula in meters per second (m/s). Thus, it is possible to express each angle, θ_i, as a function of the first incidence angle θ_1, and the respective propagation velocities (v_i, v_1):

$$\theta_i = asin\left(\frac{v_i}{v_1}\cdot\sin\theta_1\right) \tag{5}$$

Replacing equation 5 in equation 3, we get the following function, $e(\theta_1)$:

$$e(\theta_1) = d_1\cdot\tan\theta_1 + \left(\sum_{i=2}^{k} d_i\cdot\tan\left[asin\left(\frac{v_i}{v_1}\cdot\sin\theta_1\right)\right]\right) - \overline{ST^x} =$$

$$= d_1\cdot\tan\theta_1 + \left(\sum_{i=2}^{k} d_i\cdot\frac{v_i\cdot\sin\theta_1}{\sqrt{v_1^2 - v_i^2\cdot sin^2\theta_1}}\right) - \overline{ST^x} \tag{6}$$

Therefore, the ~~bisecting method~~ bisection method is applied to this function.~~,~~ Note the final form of the function, makes use of the identity: $tan\left[asin\left({}^{v_i}/_{v_1}\cdot\sin\theta_1\right)\right] = \left({}^{v_i}/_{v_1}\cdot\sin\theta_1\right)/\sqrt{1-\left({}^{v_i}/_{v_1}\cdot\sin\theta_1\right)^2} = (v_i\cdot\sin\theta_1)/\sqrt{v_1^2 - v_i^2\cdot sin^2\theta_1}$, which is only defined ~~where $-1 < (v_i/v_1)\cdot\sin\theta_1 < 1$~~ when $v_1^2 - v_i^2\cdot sin^2\theta_1 > 0$~~, since $asin(x)$ is defined for $-1 \le x \le 1$ and $tan(x)$ is continuous between $-\pi/2 < x < \pi/2$~~. This leads to determine the interval (a, b) as:

$$\left(asin\left(-\frac{v_1}{\max(v_i)}\right),\quad asin\left(\frac{v_1}{\max(v_i)}\right)\right) \tag{7}$$

$e(\theta_1)$ is a continuous function, in the interval (a, b). Figure 2 shows the typical shape of the curve associated to $e(\theta_1)$. The curve has been computed for an example multi-layered structure (Figure 1a) with 4 layers of thicknesses $d_1 = 10\text{mm}$, $d_2 = 5\text{mm}$, $d_3 = 8\text{mm}$ and $d_4 = 5\text{mm}$, where the ultrasonic propagation velocities are $v_1 = 1.5\text{mm/µs}$, $v_2 = 6\text{mm/µs}$, $v_3 = 3.1\text{mm/µs}$ and $v_4 = 5\text{mm/µs}$, respectively.

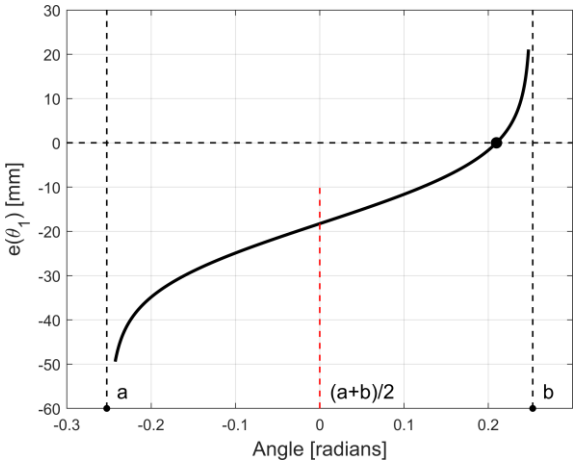

Figure 2 – Typical shape of $e(\theta_1)$.

The values $e(a)$ and $e(b)$ are of opposite sign. Thus, there is one zero crossing within the interval and the bisection method can be applied. Each iteration of the method performs these steps: (1) the midpoint of the interval $c = \frac{a+b}{2}$ is calculated, (2) the function value at the midpoint $e(c)$ is computed, (3) if convergence is

satisfactory (that is, $(c-a)$ and/or $|e(c)|$ sufficiently small), c is returned and the iteration stops; otherwise, the sign of $e(c)$ is examined and either $(a, e(a))$ or $(b, e(b))$ are replaced with $(c, e(c))$, so that there is a zero crossing within the new interval and all steps are repeated. Figure 1b illustrates the ray tracing relative to the initial guess for the zero of the function $\left(\theta_1^0 = c = \frac{a+b}{2}\right)$, the first three iterations of the method and the final result at the target, for the reference example.

4. CURVED MATERIAL INTERFACES (~~BI-DIMENSIONAL~~TWO DIMENSIONAL CASE)

Perfectly flat interfaces are only a theoretical abstraction, since real interfaces always present some degree of roughness and deviation from flatness. Moreover, intentionally curved material interfaces are often present in parts that are designed to meet critical mechanical properties. Therefore, it is necessary to generalize the formulation in Section 3, to include the possibility to solve wave propagation through multiple media, separated by curved interfaces (Figure 3a). Equation 1 is still valid for this scenario. However, the variable thickness of the material layers does not allow to compute the length of the segments $\overline{SP_1^x}$, $\overline{P_{i-1}^x P_i^x}$ and $\overline{P_{k-1}^x T^x}$ as $d_1 \cdot \tan\theta_1$, $d_i \cdot \tan\theta_i$ and $d_k \cdot \tan\theta_k$ respectively. Instead, introducing the function $f_1(x)$ to describe the curved interface between the first and second layer, the first incidence point, $P_1 \equiv \left(P_1^x, P_1^y\right)$, can be found through intersecting the propagation line in the first layer with the first interface $f_1(x)$.

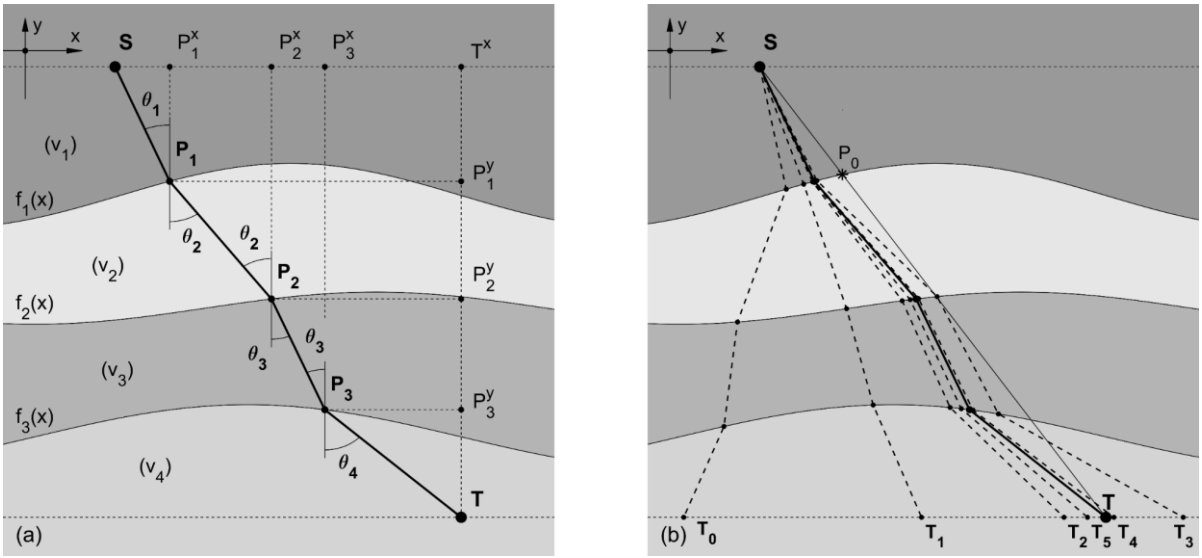

Figure 3 – Annotated ultrasonic ray tracing for multiple material layers separated by curved interfaces (a) and convergence to solution through the ~~bisecting method~~ bisection method (b).

Therefore, P_1^x and P_1^y are the solution of the system containing the equation of the line for the source S and the equation relative to the first interface, $y = f_1(x)$, as illustrated in Equation 8.

$$\begin{aligned}
&\text{if } \theta_1 \neq 0 \\
&\quad \begin{cases} line\ for\ S: & y = tan\left(\frac{\pi}{2} + \theta_1\right) \cdot (x - S^x)\ - S^y \\ first\ interface: & y = f_1(x) \end{cases} \\
&\text{else} \\
&\quad \begin{cases} line\ for\ S: & x = S^x \\ first\ interface: & y = f_1(S^x) \end{cases} \\
&\text{end}
\end{aligned} \tag{8}$$

Throughout this paper, the assumption is that each interface surface is smooth and continuous with a local radius of curvature that is many times greater than the ultrasonic wavelength. Under these conditions, a ray-based approach is valid and the problem becomes one of computing the correct ray path between source positions and target within the component. Figure 4a illustrates the refraction of an incidence wave at point P_1, on the first interface.

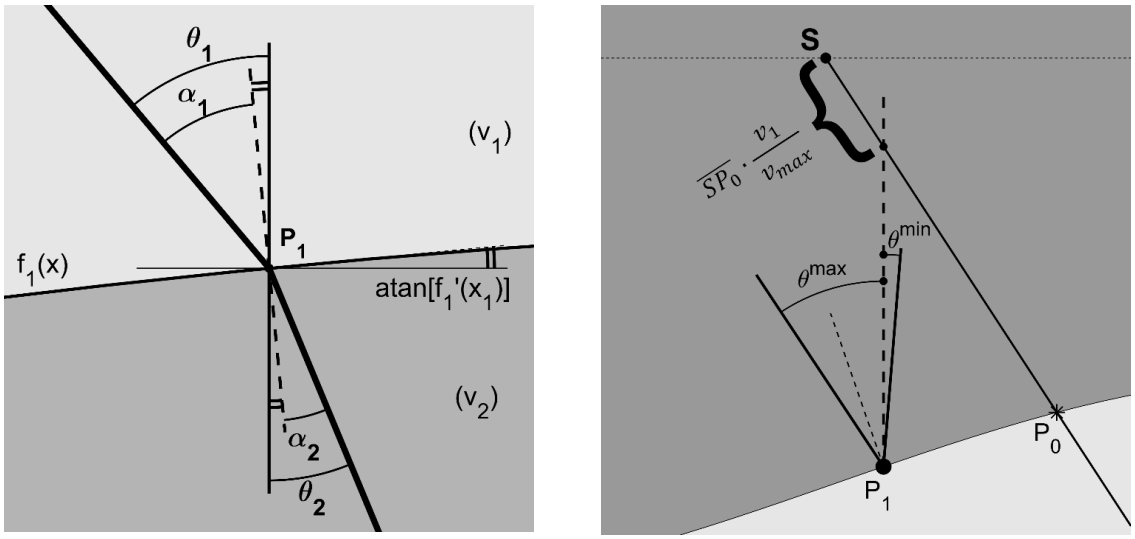

(a) (b)

Figure 4 – (a) Refraction at point $\boldsymbol{P_1}$, on the first material interface and (b) approach used for defining the initial guess point and the domain interval for $\boldsymbol{\theta_1}$.

Whereas θ_1 and θ_2 are the angles that incidence and refracted wave form with the y-axis, α_1 and α_2 are the respective angles formed with the normal to the interface at the incidence point P_1. These latter angles are constrained by the Snell's law and obey to the following equation:

$$\frac{\sin\alpha_1}{v_1} = \frac{\sin\alpha_2}{v_2} = \cdots = \frac{\sin\alpha_i}{v_i} = \frac{\sin\alpha_k}{v_k} \tag{9}$$

From Figure 4a, it is evident that:

$$\alpha_1 = \theta_1 - \text{atan}\left(f_1'(P_1^x)\right) \tag{10}$$

$$\alpha_2 = \theta_2 - \text{atan}\left(f_1'(P_1^x)\right) \tag{11}$$

Replacing Equation 10 and 11 in Equation 9, it results:

$$\theta_2 = asin\left\{\left(\frac{v_2}{v_1}\right)\cdot \sin\left[\theta_1 - atan\left(f_1'(P_1^x)\right)\right]\right\} + atan\left(f_1'(P_1^x)\right) \tag{12}$$

and generalising for the i^{th} angle (θ_i) at the i^{th} layer, and for the k^{th} angle (θ_k) at the last layer:

$$\theta_i = asin\left\{\left(\frac{v_i}{v_1}\right)\cdot \sin\left[\theta_1 - atan\left(f_1'(P_1^x)\right)\right]\right\} + atan\left(f_{i-1}'(P_{i-1}^x)\right) \tag{13}$$

$$\theta_k = asin\left\{\left(\frac{v_k}{v_1}\right)\cdot \sin\left[\theta_1 - atan\left(f_1'(P_1^x)\right)\right]\right\} + atan\left(f_{k-1}'(P_{k-1}^x)\right) \tag{14}$$

Therefore, the coordinates $\left(P_i^x, P_i^y\right)$ of the incidence points, from the 2nd to the $(k-1)^{\text{th}}$ incidence points, are the solution of the system with the equation of the line for the source P_{i-1} and the equation relative to the i^{th} interface, $y = f_i(x)$, as illustrated in Equation 15.

for i = 2:(k-1)

$$\theta_i = asin\left\{\left(\frac{v_i}{v_1}\right)\cdot \sin\left[\theta_1 - atan\left(f_1'(P_1^x)\right)\right]\right\} + atan\left(f_{i-1}'(P_{i-1}^x)\right)$$

if $\theta_i \neq 0$

$$\begin{cases} line\ for\ P_{i-1}: & y = tan\left(\frac{\pi}{2} + \theta_i\right)\cdot (x - P_{i-1}^x) - P_{i-1}^y \\ i^{th}\ interface: & y = f_i(x) \end{cases}$$

else

$$\begin{cases} line\ for\ P_{i-1}: & x = P_{i-1}^x \\ i^{th}\ interface: & y = f_i(P_{i-1}^x) \end{cases}$$

end

end (15)

Finally, the coordinates $\left(T_0^x, T_0^y\right)$ of the resulting target point related to the initial guess angle θ_1 (given as input), are the solution of the system with the equation of the line for the point P_{k-1} and the horizontal line for T ($y = T^y$), as shown in Equation 16.

$$\theta_k = asin\left\{\left(\frac{v_k}{v_1}\right)\cdot \sin\left[\theta_1 - atan\left(f_1'(P_1^x)\right)\right]\right\} + atan\left(f_{k-1}'(P_{k-1}^x)\right)$$

if $\theta_k \neq 0$

$$\begin{cases} line\ for\ P_{k-1}: & x = P_{k-1}^x + \left(P_{k-1}^y - T^y\right)\cdot \tan(\theta_k) \\ horiz.line\ for\ T: & y = T^y \end{cases}$$

else

$$\begin{cases} line\ for\ P_{k-1}: & x = P_{k-1}^x \\ horiz.line\ for\ T: & y = T^y \end{cases}$$

end (16)

Thus, the ~~bisecting method~~bisection method is applied to the error function, $e(\theta_1)$, defined as:

$$e(\theta_1) = \overline{T_j T} = T^x - T_j^x \quad (17)$$

The identification of the correct domain for $e(\theta_1)$ is crucial to make sure the application of the bisection method leads to convergence. Equations 13 and 14 are only defined where $-1 < \left(\frac{v_i}{v_1}\right)\cdot \sin\left[\theta_1 - atan\left(f_1'(P_1^x)\right)\right] < 1$. This leads to determine the interval (a, b) as:

$$(a, b) = \left(\theta^{min}, \theta^{max}\right) = \left(asin\left(-\frac{v_1}{\max(v)}\right) + atan\left(f_1'(P_1^x)\right),\quad asin\left(\frac{v_1}{\max(v)}\right) + atan\left(f_1'(P_1^x)\right)\right) \quad (18)$$

It is clear that the extremities of the interval depend on the incidence point at the first interface, since the derivative of $f_1(x)$ is computed for $x = P_1^x$ in Equation 18. In this work, the intersection between the segment $\overline{ST}$ and the first interface $f_1(x)$ is used to guide the selection of such initial guess point. Indicating with $P_0 \equiv \left(P_0^x, P_0^y\right)$ the intersection between $\overline{ST}$ and $f_1(x)$, the initial guess point is chosen as: $P_1 \equiv \left(P_1^x, P_1^y\right) \equiv \left(S^x + \frac{v_1}{v_{max}}\cdot (P_0^x - S^x)\ ,\ f_1\left(S^x + \frac{v_1}{v_{max}}\cdot (P_0^x - S^x)\right)\right)$, as it is illustrated in Figure 4b. The function values $e(a)$ and $e(b)$ are of opposite sign and there is one zero crossing within the interval. Therefore, the bisection method can be applied, following the same steps as for the case with flat interfaces until convergence is satisfactory (that is, $(c - a)$ and/or $|e(c)|$ sufficiently small), returning c and stopping iterating. Figure 3b illustrates the ray tracing relative to the initial guess $\left(\theta_1^0 = \frac{a+b}{2}\right)$, the first five iterations of the method and the final result at the target.

5. CURVED MATERIAL INTERFACES (~~TRI-DIMENSIONAL~~ THREE DIMENSIONAL CASE)

The propagation of a wave through a number (k) of material layers, separated by curved interfaces in the ~~tri-dimensional~~ three dimensional case, is the more general situation (Figure 5). Indeed, the previous ~~bi-dimensional~~ two dimensional problem can be solved as particular case of this general case. The modelling of the ~~tri-dimensional~~ three dimensional problem is the main contribution of this work.

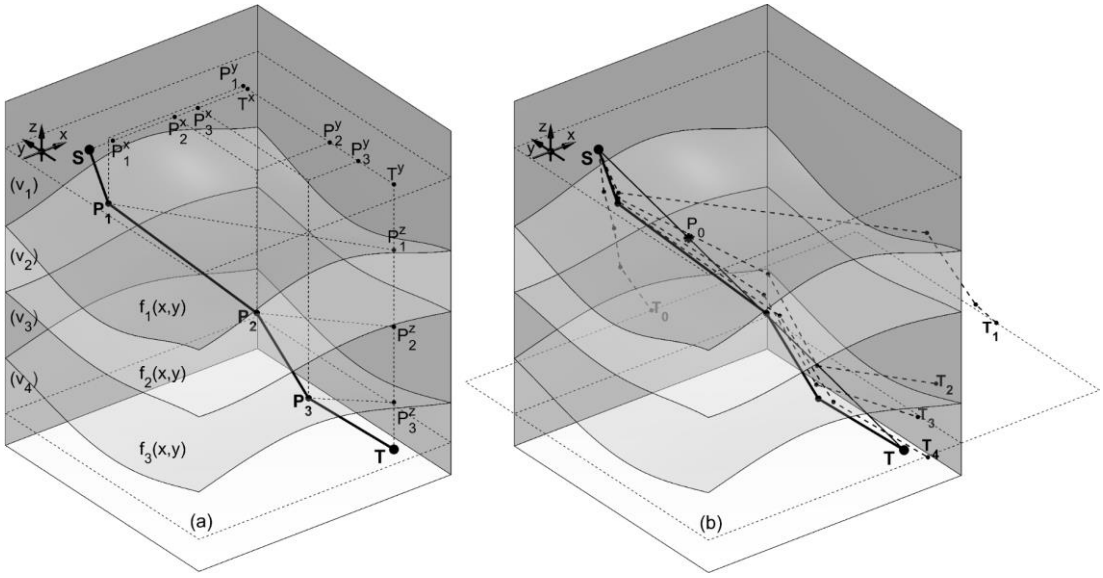

Figure 5 – Annotated ultrasonic ray tracing for multiple material layers separated by curved interfaces in the ~~tri-dimensional~~ three dimensional case (a) and convergence to solution through the ~~bisecting method~~ bisection method (b).

Introducing the function $f_1(x,y)$ to describe the curved interface surface between the first and second layer, the first incidence point, $P_1 \equiv \left(P_1^x, P_1^y, P_1^z\right)$, is the solution of the system with the Cartesian representation of the line for the source S and the equation relative to the first interface, $z = f_1(x,y)$. In the ~~tri-dimensional~~ three dimensional case it is easier to describe the direction of incidence through the unitary vector $\vec{r}_1 = \langle r_1^x, r_1^y, r_1^z \rangle$, rather than an angle θ_1. Therefore, the coordinates of the incidence point (P_1), resulting from the system illustrated, are given in Equation 19.

if $(r_1^x \neq 0, r_1^y \neq 0, r_1^z \neq 0)$

$$\begin{cases} line\ for\ S: & \begin{cases} \dfrac{x - S^x}{r_1^x} = \dfrac{y - S^y}{r_1^y} \\ \dfrac{y - S^y}{r_1^y} = \dfrac{z - S^z}{r_1^z} \end{cases} \\ first\ interface: & z = f_1(x,y) \end{cases}$$

elseif $(r_1^x = 0, r_1^y \neq 0, r_1^z \neq 0)$

$$\begin{cases} line\ for\ S: & \begin{cases} x = S^x \\ \dfrac{y - S^y}{r_1^y} = \dfrac{z - S^z}{r_1^z} \end{cases} \\ first\ interface: & z = f_1(x,y) \end{cases} \quad (19)$$

elseif $(r_1^x \neq 0, r_1^y = 0, r_1^z \neq 0)$

$$\begin{cases} line\ for\ S: & \begin{cases} y = S^y \\ \dfrac{x - S^x}{r_1^x} = \dfrac{z - S^z}{r_1^z} \end{cases} \\ first\ interface: & z = f_1(x,y) \end{cases}$$

elseif $(r_1^x \neq 0, r_1^y \neq 0, r_1^z = 0)$

$$\begin{cases} line\ for\ S: & \begin{cases} z = S^z \\ \dfrac{x - S^x}{r_1^x} = \dfrac{y - S^y}{r_1^y} \end{cases} \\ first\ interface: & z = f_1(x,y) \end{cases}$$

elseif $(r_1^x = 0, r_1^y = 0, r_1^z \neq 0)$

$$\begin{cases} line\ for\ S: & \begin{cases} x = S^x \\ y = S^y \end{cases} \\ first\ interface: & z = f_1(x,y) \end{cases}$$

elseif $(r_1^x = 0, r_1^y \neq 0, r_1^z = 0)$

$$\begin{cases} line\ for\ S: & \begin{cases} x = S^x \\ z = S^z \end{cases} \\ first\ interface: & z = f_1(x,y) \end{cases}$$

elseif $(r_1^x \neq 0, r_1^y = 0, r_1^z = 0)$

$$\begin{cases} line\ for\ S: & \begin{cases} y = S^y \\ z = S^z \end{cases} \\ first\ interface: & z = f_1(x,y) \end{cases}$$

end

Rewriting the equation relative to the first interface, $z = f_1(x,y)$, as $f_1(x,y,z) = 0$, the unit normal vector to the surface at the point P_1 is given by $\vec{\boldsymbol{n}}_1 = \nabla \boldsymbol{f_1}(P_1) / \|\nabla \boldsymbol{f_1}(P_1)\|$.

$$\vec{\boldsymbol{n}}_1 = \frac{\nabla \boldsymbol{f}_1(P_1)}{\|\nabla \boldsymbol{f}_1(P_1)\|} = \frac{\langle \frac{\partial f_1}{\partial x}(P_1^x, P_1^y, P_1^z), \frac{\partial f_1}{\partial y}(P_1^x, P_1^y, P_1^z), \frac{\partial f_1}{\partial z}(P_1^x, P_1^y, P_1^z) \rangle}{\sqrt{\frac{\partial f_1}{\partial x}(P_1^x, P_1^y, P_1^z)^2 + \frac{\partial f_1}{\partial y}(P_1^x, P_1^y, P_1^z)^2 + \frac{\partial f_1}{\partial z}(P_1^x, P_1^y, P_1^z)^2}} = \langle n_1^x, n_1^y, n_1^z \rangle \quad (20)$$

Considering the refraction at the first interface, the unitary vector for the direction ($\vec{\boldsymbol{r}}_2$) of the refracted wave in the second layer ~~lays on~~ lies in the plane π_1, which also contains the vectors $\vec{\boldsymbol{r}}_1$ and $\vec{\boldsymbol{n}}_1$. Figure 6 introduces the notation of the geometric entities used to compute the refraction direction.

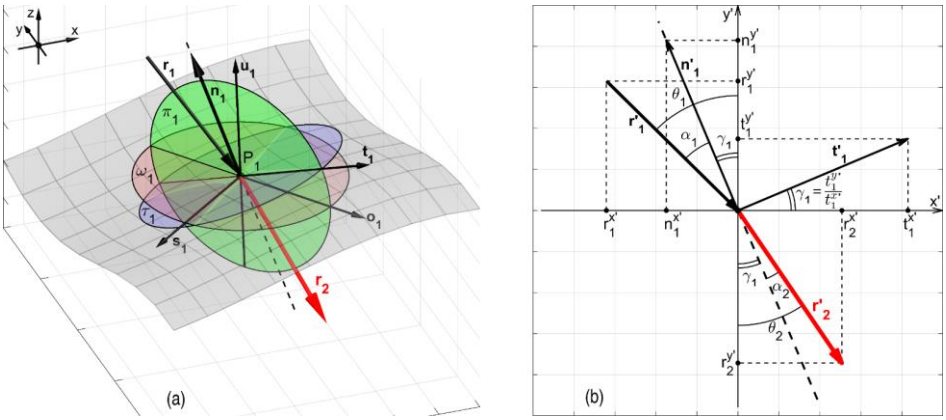

Figure 6 – (a) Refraction in ~~tri-dimensional~~three dimensional space and (b) projection onto the plane $\boldsymbol{x'}$-$\boldsymbol{y'}$ ($\boldsymbol{\pi_1}$).

The planes ~~ω_1~~ ω_1 is the horizontal plane that passes through P_1 and has normal vector $[0 \quad 0 \quad 1]^T$, which is the plane described by the equation: $z = f_1(P_1)$. The plane ~~and~~ τ_1 ~~is are, respectively, the horizontal plane for P_1 and~~ the plane tangent to the surface $f_1(x,y,z) = 0$ in P_1, whose normal coincides with $\vec{\boldsymbol{n}}_1$. The direction resulting from the intersection between π_1 and ω_1 is indicated by the unitary vector $\vec{\boldsymbol{o}}_1$. Instead, $\vec{\boldsymbol{t}}_1$ is the unitary vector resulting from the intersection between π_1 and τ_1. Finally, the unitary vector perpendicular to π_1 is indicated with $\vec{\boldsymbol{s}}_1$ and the vector perpendicular to $\vec{\boldsymbol{s}}_1$ and $\vec{\boldsymbol{o}}_1$ is designated by $\vec{\boldsymbol{u}}_1$. Mathematically, the components of these vectors are computed through the following equations:

$$\vec{s}_1 = \vec{n}_{1P_x} \times \vec{r}_1 = \begin{pmatrix} r_1^z n_1^y - r_1^y n_1^z \\ r_1^x n_1^z - r_1^z n_1^x \\ r_1^y n_1^x - r_1^x n_1^y \end{pmatrix} = \begin{pmatrix} s_1^x \\ s_1^y \\ s_1^z \end{pmatrix} \tag{21}$$

$$\vec{o}_1 = \begin{pmatrix} 0 \\ 0 \\ 1 \end{pmatrix} \times \vec{s}_1 = \begin{pmatrix} r_1^z n_1^x - r_1^x n_1^z \\ r_1^z n_1^y - r_1^y n_1^z \\ 0 \end{pmatrix} = \begin{pmatrix} o_1^x \\ o_1^y \\ o_1^z \end{pmatrix} \tag{22}$$

$$\vec{t}_1 = \vec{s}_1 \times \vec{n}_{1P_x} = \begin{pmatrix} n_1^z(r_1^x n_1^z - r_1^z n_1^x) - n_1^y(r_1^y n_1^x - r_1^x n_1^y) \\ n_1^x(r_1^y n_1^x - r_1^x n_1^y) - n_1^z(r_1^z n_1^y - r_1^y n_1^z) \\ n_1^y(r_1^z n_1^y - r_1^y n_1^z) - n_1^x(r_1^x n_1^z - r_1^z n_1^x) \end{pmatrix} = \begin{pmatrix} t_1^x \\ t_1^y \\ t_1^z \end{pmatrix} \tag{23}$$

$$\vec{u}_1 = \vec{s}_1 \times \vec{o}_1 = \begin{pmatrix} (r_1^x n_1^y - r_1^y n_1^x)(r_1^z n_1^y - r_1^y n_1^z) \\ (r_1^y n_1^x - r_1^x n_1^y)(r_1^z n_1^x - r_1^x n_1^z) \\ (r_1^z n_1^y - r_1^y n_1^z)^2 + (r_1^x n_1^z - r_1^z n_1^x)^2 \end{pmatrix} = \begin{pmatrix} u_1^x \\ u_1^y \\ u_1^z \end{pmatrix} \tag{24}$$

Therefore, it is possible to define the rotational matrix $\boldsymbol{R_1}$, which is used to transform the vectors $\vec{\boldsymbol{r}}_1$, $\vec{\boldsymbol{n}}_1$ and $\vec{\boldsymbol{t}}_1$ in the rotated vectors $\vec{\boldsymbol{r}}'_1$, $\vec{\boldsymbol{n}}'_1$ and $\vec{\boldsymbol{t}}'_1$.

$$\boldsymbol{R_1} = [\vec{o}_1 \quad \vec{u}_1 \quad \vec{s}_1] = \begin{bmatrix} o_1^x & u_1^x & s_1^x \\ o_1^y & u_1^y & s_1^y \\ o_1^z & u_1^z & s_1^z \end{bmatrix} \tag{25}$$

$$\vec{r}'_1 = \vec{r}_1 \cdot \boldsymbol{R_1} = \begin{pmatrix} r_1^x \\ r_1^y \\ r_1^z \end{pmatrix}^{\boldsymbol{T}} \cdot \begin{bmatrix} o_1^x & u_1^x & s_1^x \\ o_1^y & u_1^y & s_1^y \\ o_1^z & u_1^z & s_1^z \end{bmatrix} = \begin{pmatrix} r_1^x o_1^x + r_1^y o_1^y + r_1^z o_1^z \\ r_1^x u_1^x + r_1^y u_1^y + r_1^z u_1^z \\ r_1^x s_1^x + r_1^y s_1^y + r_1^z s_1^z \end{pmatrix} = \begin{pmatrix} r_1^{x'} \\ r_1^{y'} \\ r_1^{z'} \end{pmatrix} = \tag{26}$$

$$= \begin{pmatrix} r_1^x r_1^z n_1^x - (r_1^x)^2 n_1^z + r_1^y r_1^z n_1^y - (r_1^y)^2 n_1^z \\ (r_1^x)^2 r_1^z (n_1^y)^2 - 2r_1^x r_1^y r_1^z n_1^x n_1^y + (r_1^y)^2 r_1^z (n_1^x)^2 + (r_1^z)^3 (n_1^y)^2 - 2r_1^y (r_1^z)^2 n_1^y n_1^z + (r_1^y)^2 r_1^z (n_1^z)^2 + (r_1^x)^2 r_1^z (n_1^z)^2 - 2r_1^x (r_1^z)^2 n_1^x n_1^z + (r_1^z)^3 (n_1^x)^2 \\ 0 \end{pmatrix}$$

$$\vec{n}'_1 = \vec{n}_1 \cdot \boldsymbol{R_1} = \begin{pmatrix} n_1^x \\ n_1^y \\ n_1^z \end{pmatrix}^{T} \cdot \begin{bmatrix} o_1^x & u_1^x & s_1^x \\ o_1^y & u_1^y & s_1^y \\ o_1^z & u_1^z & s_1^z \end{bmatrix} = \begin{pmatrix} n_1^x o_1^x + n_1^y o_1^y + n_1^z o_1^z \\ n_1^x u_1^x + n_1^y u_1^y + n_1^z u_1^z \\ n_1^x s_1^x + n_1^y s_1^y + n_1^z s_1^z \end{pmatrix} = \begin{pmatrix} n_1^{x'} \\ n_1^{y'} \\ n_1^{z'} \end{pmatrix} = \tag{27}$$

$$= \begin{pmatrix} r_1^z (n_1^x)^2 - r_1^x n_1^x n_1^z - r_1^y n_1^y n_1^z + r_1^z (n_1^y)^2 \\ (r_1^x)^2 (n_1^y)^2 n_1^z - 2r_1^x r_1^y n_1^x n_1^y n_1^z + (r_1^y)^2 (n_1^x)^2 n_1^z + (r_1^z)^2 (n_1^y)^2 n_1^z - 2r_1^y r_1^z n_1^y (n_1^z)^2 + (r_1^y)^2 (n_1^z)^3 + (r_1^x)^2 (n_1^z)^3 - 2r_1^x r_1^z n_1^x (n_1^z)^2 + (r_1^z)^2 (n_1^x)^2 n_1^z \\ 0 \end{pmatrix}$$

$$\vec{t}'_1 = \vec{t}_1 \cdot \boldsymbol{R_1} = \begin{pmatrix} t_1^x \\ t_1^y \\ t_1^z \end{pmatrix}^{T} \cdot \begin{bmatrix} o_1^x & u_1^x & s_1^x \\ o_1^y & u_1^y & s_1^y \\ o_1^z & u_1^z & s_1^z \end{bmatrix} = \begin{pmatrix} t_1^x o_1^x + t_1^y o_1^y + t_1^z o_1^z \\ t_1^x u_1^x + t_1^y u_1^y + t_1^z u_1^z \\ t_1^x s_1^x + t_1^y s_1^y + t_1^z s_1^z \end{pmatrix} = \begin{pmatrix} t_1^{x'} \\ t_1^{y'} \\ t_1^{z'} \end{pmatrix} = \tag{28}$$

$$= \begin{pmatrix} -(r_1^x)^2 (n_1^y)^2 n_1^z + 2r_1^x r_1^y n_1^x n_1^y n_1^z - (r_1^y)^2 (n_1^x)^2 n_1^z - (r_1^z)^2 (n_1^y)^2 n_1^z + 2r_1^y r_1^z n_1^y (n_1^z)^2 - (r_1^y)^2 (n_1^z)^3 - (r_1^x)^2 (n_1^z)^3 + 2r_1^x r_1^z n_1^x (n_1^z)^2 - (r_1^z)^2 (n_1^x)^2 n_1^z \\ r_1^z (n_1^x)^2 - r_1^x n_1^x n_1^z - r_1^y n_1^y n_1^z + r_1^z (n_1^y)^2 \\ 0 \end{pmatrix}$$

Since $r_1^{z'} = n_1^{z'} = t_1^{z'} = 0$, the rotated vectors can be represented on the $x'y'$-plane, where the imposition of ~~the~~ Snell's law is brought back to the ~~bidimensional~~ two dimensional domain, as illustrated in Figure 6b. Beside the sign, the angle formed by $\vec{\boldsymbol{t}}'_1$ with the x'-axis is equal to the angle formed by $\vec{\boldsymbol{n}}'_i$ with the y'-axis. Thus, this angle is indicated with $\gamma_1 = atan\left(t_1^{y'}/t_1^{x'}\right) = -atan\left(n_1^{x'}/n_1^{y'}\right)$. Therefore, rewriting Equations (13) and (14), which originate from ~~the~~ Snell's law, using γ_1 in place of $atan\left(f'_1(P_1^x)\right)$, the angle formed by the rotated refracted vector ($\vec{\boldsymbol{r}}'_1$) with the y'-axis results:

$$\theta_2 = asin\left\{\left(\frac{v_2}{v_1}\right) \cdot \sin\left[\theta_1 + atan\left(\frac{n_1^{x'}}{n_1^{y'}}\right)\right]\right\} - atan\left(\frac{n_1^{x'}}{n_1^{y'}}\right), \qquad \text{with: } \theta_1 = -atan\left(\frac{r_1^{x'}}{r_1^{y'}}\right) \tag{29}$$

Thus, the components of the unitary vector $\vec{\boldsymbol{r}}'_2$ in the two dimensional ~~bidimensional~~ domain and the components of $\vec{\boldsymbol{r}}_2$ in the original ~~tri-dimensional~~three dimensional space are respectively:

$$\vec{\boldsymbol{r}}'_2 = \begin{pmatrix} r_2^{x'} \\ r_2^{y'} \end{pmatrix} = \begin{pmatrix} \sin(\theta_2) \\ -\cos(\theta_2) \end{pmatrix} \tag{30}$$

$$\vec{\boldsymbol{r}}_2 = \begin{pmatrix} r_2^{x'} \\ r_2^{y'} \\ 0 \end{pmatrix}^T \cdot \boldsymbol{R}^{-1} = \begin{pmatrix} \sin(\theta_2) \\ -\cos(\theta_2) \\ 0 \end{pmatrix}^T \cdot \begin{bmatrix} o_1^x & u_1^x & s_1^x \\ o_1^y & u_1^y & s_1^y \\ o_1^z & u_1^z & s_1^z \end{bmatrix}^{-1} = \begin{pmatrix} \sin(\theta_2)\, o_1^x - \cos(\theta_2) o_1^y \\ \sin(\theta_2)\, u_1^x - \cos(\theta_2)\, u_1^y \\ \sin(\theta_2)\, s_1^x - \cos(\theta_2)\, s_1^y \end{pmatrix} \tag{31}$$

Generalising for the refracted direction in any i^{th} layer ($\vec{\boldsymbol{r}}_{\text{i}}$) and in the last layer ($\vec{\boldsymbol{r}}_{\text{k}}$):

$$\vec{\boldsymbol{r}}_i = \begin{pmatrix} \sin(\theta_i)\, o_{i-1}^x - \cos(\theta_i) o_{i-1}^y \\ \sin(\theta_i)\, u_{i-1}^x - \cos(\theta_i)\, u_{i-1}^y \\ \sin(\theta_i)\, s_{i-1}^x - \cos(\theta_i)\, s_{i-1}^y \end{pmatrix}, \quad \text{with:} \quad \theta_i = asin\left\{\left(\frac{v_i}{v_1}\right) \cdot \sin\left[\theta_1 + atan\left(\frac{n_1^{x'}}{n_1^{y'}}\right)\right]\right\} - atan\left(\frac{n_{i-1}^{x'}}{n_{i-1}^{y'}}\right) \tag{32}$$

$$\vec{\boldsymbol{r}}_k = \begin{pmatrix} \sin(\theta_k)\, o_{k-1}^x - \cos(\theta_k) o_{k-1}^y \\ \sin(\theta_k)\, u_{k-1}^x - \cos(\theta_k)\, u_{k-1}^y \\ \sin(\theta_k)\, s_{k-1}^x - \cos(\theta_k)\, s_{k-1}^y \end{pmatrix}, \quad \text{with:} \quad \theta_k = asin\left\{\left(\frac{v_k}{v_1}\right) \cdot \sin\left[\theta_1 + atan\left(\frac{n_1^{x'}}{n_1^{y'}}\right)\right]\right\} - atan\left(\frac{n_{k-1}^{x'}}{n_{k-1}^{y'}}\right) \tag{33}$$

Therefore, the coordinates $\left(P_i^x, P_i^y\right)$ of the incidence points, from the 2nd to the $(k-1)^{\text{th}}$ incidence points, are the solution of the system with the equation of the line for the source P_{i-1}, whose direction is given by the unitary vector ($\vec{\boldsymbol{r}}_i$), and the equation relative to the i^{th} interface, $z = f_i(x, y)$~~.~~. This system of equations is given in Appendix A. ~~as illustrated in Equation 34.~~ Finally, the coordinates $\left(T_0^x, T_0^y, T_0^z\right)$ of the resulting target point related to the initial guess angle θ_1 (given as input), are the solution of the system containing the equation of the line for the point P_{k-1} and the horizontal plane for T ($z = T^z$), as shown given in Appendix B.~~Equation 35.~~

Thus, the ~~bisecting method~~bisection method is applied to the two error functions, $e_x(\vec{\boldsymbol{r}}_1)$ and $e_y(\vec{\boldsymbol{r}}_1)$, defined as:

$$\begin{aligned} e_x(\vec{\boldsymbol{r}}_1) &= T^x - T_j^x \\ e_y(\vec{\boldsymbol{r}}_1) &= T^y - T_j^y \end{aligned} \tag{34}$$

As in the ~~bi-dimensional~~two dimensional case, it is crucial to determine the limits of the domain of these error functions to make sure the application of the bisection method leads to convergence. This means defining the interval for the components of the vector $\vec{\boldsymbol{r}}_1 = \langle r_1^x, r_1^y, r_1^z \rangle$. As $\theta_1 = -atan\left(r_1^{x'}/r_1^{y'}\right)$, Equations 32 and 33 are only defined where $-1 < \left(\frac{v_i}{v_1}\right) \cdot sin\left[-atan\left(r_1^{x'}/r_1^{y'}\right) + atan\left(n_1^{x'}/n_1^{y'}\right)\right] < 1$. The following system brings together this latter condition and imposes the unitary modulus.

$$\begin{cases} -1 < \left(\frac{v_i}{v_1}\right) \cdot sin\left[-atan\left(\frac{r_1^{x'}}{r_1^{y'}}\right) + atan\left(\frac{n_1^{x'}}{n_1^{y'}}\right)\right] < 1 \\ \|\vec{\boldsymbol{r}}_1\| = 0 \end{cases}$$

$$\begin{cases} -1 < \left(\frac{v_i}{v_1}\right) \cdot \sin\left[-atan\left(\frac{r_1^x r_1^z n_1^x - (r_1^x)^2 n_1^z + r_1^y r_1^z n_1^y - (r_1^y)^2 n_1^z}{(r_1^x)^2 r_1^z (n_1^y)^2 - 2 r_1^x r_1^y r_1^z n_1^x n_1^y + (r_1^y)^2 r_1^z (n_1^x)^2 + (r_1^z)^3 (n_1^y)^2 - 2 r_1^y (r_1^z)^2 n_1^y n_1^z + (r_1^y)^2 r_1^z (n_1^z)^2 + (r_1^x)^2 r_1^z (n_1^z)^2 - 2 r_1^x (r_1^z)^2 n_1^x n_1^z + (r_1^z)^3 (n_1^x)^2}\right) + \right. \\ \left. \quad + atan\left(\frac{r_1^z (n_1^x)^2 - r_1^x n_1^x n_1^z - r_1^y n_1^y n_1^z + r_1^z (n_1^y)^2}{(r_1^x)^2 (n_1^y)^2 n_1^z - 2 r_1^x r_1^y n_1^x n_1^y n_1^z + (r_1^y)^2 (n_1^x)^2 n_1^z + (r_1^z)^2 (n_1^y)^2 n_1^z - 2 r_1^y r_1^z n_1^y (n_1^z)^2 + (r_1^y)^2 (n_1^z)^3 + (r_1^x)^2 (n_1^z)^3 - 2 r_1^x r_1^z n_1^x (n_1^z)^2 + (r_1^z)^2 (n_1^z)^2 n_1^z}\right)\right] < 1 \\ (r_1^x)^2 + (r_1^y)^2 + (r_1^z)^2 = 1 \end{cases} \tag{35}$$

Unfortunately, after replacing $r_1^{x'}$, $r_1^{y'}$, $n_1^{x'}$ and $n_1^{y'}$ with their respective expressions from Equation 26 and 27, which are functions of the sought values r_1^x, r_1^y and r_1^z, it is not easy to isolate their domain intervals. In this work an alternative route is found and the domain intervals are approximated by building on the formulation for the two dimensional ~~bidimensional~~ case. The first two inequalities in the following system derive~~are, respectively, corresponding to~~ from the first inequality in Equation 35~~34)~~, respectively written for the x-z plane and the y-z plane, where the ratio $n_1^{x\prime}/n_1^{y\prime}$ is replaced with the partial derivatives of the first interface function for x and y (computed in P_1).

$$\begin{cases} -1 < \left(\frac{v_i}{v_{max}}\right) \cdot \sin\left[-atan\left(\frac{r_1^x}{r_1^z}\right) - atan\left(\frac{\partial f_1}{\partial x}(P_1^x, P_1^y, P_1^z)\right)\right] < 1 \\ -1 < \left(\frac{v_i}{v_{max}}\right) \cdot \sin\left[-atan\left(\frac{r_1^y}{r_1^z}\right) - atan\left(\frac{\partial f_1}{\partial y}(P_1^x, P_1^y, P_1^z)\right)\right] < 1 \\ (r_1^x)^2 + (r_1^y)^2 + (r_1^z)^2 = 1 \\ -tan\left[asin\left(\frac{v_1}{v_{max}}\right) + atan\left(\frac{\partial f_1}{\partial x}(P_1^x, P_1^y, P_1^z)\right)\right] < \frac{r_1^x}{r_1^z} < tan\left[asin\left(\frac{v_1}{v_{max}}\right) - atan\left(\frac{\partial f_1}{\partial x}(P_1^x, P_1^y, P_1^z)\right)\right] \\ -tan\left[asin\left(\frac{v_1}{v_{max}}\right) + atan\left(\frac{\partial f_1}{\partial y}(P_1^x, P_1^y, P_1^z)\right)\right] < \frac{r_1^y}{r_1^z} < tan\left[asin\left(\frac{v_1}{v_{max}}\right) - atan\left(\frac{\partial f_1}{\partial y}(P_1^x, P_1^y, P_1^z)\right)\right] \\ r_1^z = -\sqrt{\frac{1}{\left(\frac{r_1^x}{r_1^z}\right)^2 + \left(\frac{r_1^y}{r_1^z}\right)^2 + 1}} \end{cases} \tag{36}$$

Isolating the ratios r_1^x/r_1^z and r_1^y/r_1^z from the first two inequalities and expressing r_1^z as a function of such ratios, from the unitary modulus condition, leads to obtaining the lower and upper domain interval values for the components of $\vec{\boldsymbol{r}}_1$, which are respectively a^x, a^y, a^z and b^x, b^y and b^z, as given in (37).

$$\begin{pmatrix} a^x \\ a^y \\ a^z \end{pmatrix} = \begin{pmatrix} -tan\left[asin\left(\frac{v_1}{v_{max}}\right) - atan\left(\frac{\partial f_1}{\partial x}(P_1)\right)\right] \cdot \left\{\left(tan\left[asin\left(\frac{v_1}{v_{max}}\right) - atan\left(\frac{\partial f_1}{\partial x}(P_1)\right)\right]\right)^2 + \left(tan\left[asin\left(\frac{v_1}{v_{max}}\right) - atan\left(\frac{\partial f_1}{\partial y}(P_1)\right)\right]\right)^2 + 1\right\}^{-\frac{1}{2}} \\ -tan\left[asin\left(\frac{v_1}{v_{max}}\right) - atan\left(\frac{\partial f_1}{\partial y}(P_1)\right)\right] \cdot \left\{\left(tan\left[asin\left(\frac{v_1}{v_{max}}\right) - atan\left(\frac{\partial f_1}{\partial x}(P_1)\right)\right]\right)^2 + \left(tan\left[asin\left(\frac{v_1}{v_{max}}\right) - atan\left(\frac{\partial f_1}{\partial y}(P_1)\right)\right]\right)^2 + 1\right\}^{-\frac{1}{2}} \\ -\left\{\left(tan\left[asin\left(\frac{v_1}{v_{max}}\right) - atan\left(\frac{\partial f_1}{\partial x}(P_1)\right)\right]\right)^2 + \left(tan\left[asin\left(\frac{v_1}{v_{max}}\right) - atan\left(\frac{\partial f_1}{\partial y}(P_1)\right)\right]\right)^2 + 1\right\}^{-\frac{1}{2}} \end{pmatrix}$$

$$\begin{pmatrix} b^x \\ b^y \\ b^z \end{pmatrix} = \begin{pmatrix} tan\left[asin\left(\frac{v_1}{v_{max}}\right) + atan\left(\frac{\partial f_1}{\partial x}(P_1)\right)\right] \cdot \left\{\left(tan\left[asin\left(\frac{v_1}{v_{max}}\right) + atan\left(\frac{\partial f_1}{\partial x}(P_1)\right)\right]\right)^2 + \left(tan\left[asin\left(\frac{v_1}{v_{max}}\right) + atan\left(\frac{\partial f_1}{\partial y}(P_1)\right)\right]\right)^2 + 1\right\}^{-\frac{1}{2}} \\ tan\left[asin\left(\frac{v_1}{v_{max}}\right) + atan\left(\frac{\partial f_1}{\partial y}(P_1)\right)\right] \cdot \left\{\left(tan\left[asin\left(\frac{v_1}{v_{max}}\right) + atan\left(\frac{\partial f_1}{\partial x}(P_1)\right)\right]\right)^2 + \left(tan\left[asin\left(\frac{v_1}{v_{max}}\right) + atan\left(\frac{\partial f_1}{\partial y}(P_1)\right)\right]\right)^2 + 1\right\}^{-\frac{1}{2}} \\ -\left\{\left(tan\left[asin\left(\frac{v_1}{v_{max}}\right) + atan\left(\frac{\partial f_1}{\partial x}(P_1)\right)\right]\right)^2 + \left(tan\left[asin\left(\frac{v_1}{v_{max}}\right) + atan\left(\frac{\partial f_1}{\partial y}(P_1)\right)\right]\right)^2 + 1\right\}^{-\frac{1}{2}} \end{pmatrix} \tag{37}$$

It is clear that the extremities of the interval depend on the incidence point at the first interface, since the partial derivatives of the first interface function, $\frac{\partial f_1}{\partial x}(x,y)$ and $\frac{\partial f_1}{\partial y}(x,y)$, are computed for $(x,y) = \left(P_1^x, P_1^y\right)$. Therefore, the choice of the initial guess for P_1 is critical to ensure the convergence to the root solution, through the bisection method. Following the same approach used for the two dimensional ~~bidimensional~~ case, the intersection between the segment $\overline{ST}$ and the first interface $f_1(x,y)$ is used to guide the selection of ~~such~~the initial guess point. Indicating with $P_0 \equiv \left(P_0^x, P_0^y, P_0^z\right)$ the intersection between $\overline{ST}$ and $f_1(x,y)$, the initial guess point is chosen as:

$$P_1 \equiv \begin{pmatrix} P_1^x \\ P_1^y \\ P_1^z \end{pmatrix} \equiv \begin{pmatrix} S^x + \frac{v_1}{v_{max}} \cdot (P_0^x - S^x) \\ S^y + \frac{v_1}{v_{max}} \cdot (P_0^y - S^y) \\ f_1\left(S^x + \frac{v_1}{v_{max}} \cdot (P_0^x - S^x), S^y + \frac{v_1}{v_{max}} \cdot (P_0^y - S^y)\right) \end{pmatrix} \tag{38}$$

Therefore, the bisection method can be applied, following the same steps as for the case with flat interfaces until convergence is satisfactory (that is, $(c^x - a^x)$, $(c^y - a^y)$, $(c^z - a^z)$ and/or $|e_x(c)|$ and $|e_y(c)|$ sufficiently small), returning $\vec{\boldsymbol{r}}_1 = \langle c^x, c^y, c^z \rangle$ and stopping iterating. Figure 5b illustrates the ray tracing relative to the initial guess for $\vec{\boldsymbol{r}}_1$, the first four iterations of the method and the final~~e~~ solution at the target.

6. APPLICATION EXAMPLES

The proposed mathematical model can be applied to several scenarios, to enable accurate ultrasound ray tracing and improve ultrasonic inspection. Multi-layered structures, such as composite parts and coated components, are becoming common in many fields, since they are appreciated for their unique mechanical properties. Also, any ultrasonic inspection performed through embedding the probe within a coupling wheel, whose rubber tyre has a significant velocity mismatch with either internal or external media (i.e. designed to withstand temperatures rather than optimal acoustic matching), should be considered as a multi-layered inspection [19]. The ~~tri-dimensional~~ three dimensional tracing of ultrasonic rays is often approximated in these situations, with the result of compromising the effectiveness of ultrasonic inspection techniques used to detect cracks and defects. Robotic inspection systems have been developed in recent years to speed up the inspection of large parts made of composite materials [8, 20]. A robot manipulator usually moves an ultrasonic phased array probe along the contour of a surface, while pulse-echo signals are collected. However, when parts are thick and/or their thickness is variable, it is necessary to employ two manipulators, the first for holding the generating ultrasonic probe from one side of the part and the second for receiving the signal from the other side of the component respectively [21]. The presented mathematical model can be used to compute the direction of the transmitted ultrasonic ray, thus optimizing the orientation of the receiving transducer throughout the inspection of such complex geometries. The capability of the model to work in the ~~tri-dimensional~~ three dimensional space makes it suitable to be used for challenging-to-inspect parts with complex geometries.

For the sake of presenting a practical application example of the model, the remaining part of this paper focuses on the field of in-process ultrasonic inspection of welded plates. Non-destructive evaluation (NDE) in the form of UT testing has become the industrial standard for welds to be tested in a safe, efficient and unobtrusive manner. Traditionally, fusion welding and NDE of welds are separate processes in the supply chain, which ultimately limit productivity, throughput and increase rework. Therefore, researchers are currently working hard to combine both of these practices directly at the point of manufacture through the use of new inspection, automation and control approaches [22-26]. The concept of inspecting the welding process in real-time offers the possibility to control, adapt and consistently ensure high-quality defect-free welding. Early detection of defects, in high-value thick complex welded components, would result in reduced rework requirements and hence improved component build time and overall cost. Inspection of each pass during the welding process would allow the early and efficient screening of each layer and detection of any flaws [23]. However, ultrasonic ~~inspecting~~ inspection of the welds at the point of manufacture is challenging, due to the high temperature of the welded parts. The speed of sound in a material changes with its temperature. Javadi et al. [23] demonstrated that the ultrasonic inspection results can be considerably influenced by the temperature. For example, a defect can be located with a position mismatch of up to 3 mm in two inspections carried out at 28° C and 164° C. Mild steel melts at around 1370 degrees C. Therefore, welded parts at the point of manufacture present a temperature gradient, with temperatures rising from room temperature to several hundreds of degrees C (depending on the time elapsed from the deposit of the welding material). It is notoriously difficult to predict the path that an ultrasound ray follows from a source to a target point, when it travels through a material with non-constant temperatures. This could be computed through Finite Element Modelling (FEM), but thermo-mechanic FEM simulations are usually very resource-demanding and time-consuming. This section demonstrates how the presented mathematical model can be used to

approximate the ultrasonic paths, by discretizing the material of a welded plate with a succession of constant temperature regions. Figure 7a shows the reference case used herein. The sample under consideration is a 15mm thick steel specimen with a 60 degrees single V-groove weld. Two mild steel 15mm thick plates are supposed to be butt-welded and the temperature of the deposited material is supposed to have cooled for 6 minutes after completion of the weld process. In order to consider the thermal distribution in the weldment, and the associated spatial variation in elastic properties, a finite element (FE)-derived thermal distribution map obtained from a weld model was corroborated experimentally using thermocouple measurements [27]. The resultant map comprises eleven temperature zones across the specimen, with relative sound speed in the material, to represent the effect of temperature variation on wave propagation.

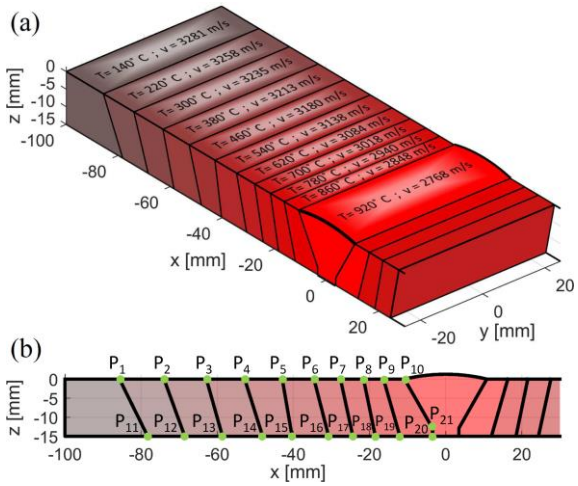

Figure 7 – (a) Discretization of welded plate through eleven regions with constant temperature~~, (b) representation of isothermal interfaces~~ and (b~~c~~) transversal section with key points used for computation of analytical surfaces.

Figure 7b gives a transversal section of such interfaces, with the key points used to express the interfaces as analytical surfaces. Although ~~the authors of~~ this work ~~want to demonstrate the use of the~~ introduced the generalised mathematical model of Snell's law for curved material interfaces (the ~~tri dimensional~~three dimensional case, described in Section 5), the observant reader will realize that any evolution of the temperature in the y-direction is neglected in this example. This is just for the sake of clarity, to make the example and the following figures more easily comprehensible.

The i[th] horizontal superficial interface at the top of the welded plate, between the points P_i and P_{i+1}, is represented analytically by the function:

$$z = f(x,y) = z_{P_i} \;\; ; \quad \text{for:} \begin{cases} x_{P_i} < x < x_{P_{i+1}} \\ -\infty < y < \infty \end{cases} . \tag{39}$$

The i[th] volumetric tilted interface, between the points P_i and P_{i+10}, is represented analytically by the function:

$$z = f(x,y) = mx + b \;\; ; \quad \text{with:} \begin{cases} m = \frac{z_{P_{i+10}} - z_{P_i}}{x_{P_{i+10}} - x_{P_i}} \\ b = -m * x_{P_i} \end{cases} ; \quad \text{for:} \begin{cases} x_{P_i} < x < x_{P_{i+10}} \\ -\infty < y < \infty \end{cases} . \tag{40}$$

Finally, the vertical surface corresponding to the root face at the bottom of the bevel is given analytically by the following function:

$$x = f(y,z) = x_{P_{20}} \;\; ; \quad \text{for:} \begin{cases} -\infty < y < \infty \\ z_{P_{20}} < z < z_{P_{21}} \end{cases} . \tag{41}$$

While straight beam techniques can be highly effective at finding laminar flaws, they are not effective when testing many common welds, where discontinuities are typically not oriented parallel to the surface of the welded plates. The combination of weld geometry, the orientation of flaws, and the presence of the weld crown or bead require inspection from the side of the weld using a beam generated at an angle. Angle beam testing is by far the most commonly used technique in ultrasonic flaw detection in butt welds [28-30]. Angle beam probes consist of a transducer and a wedge. They use the principle of refraction and mode conversion at a boundary to produce refracted shear waves in the test piece [31, 32]. When using wide phased array probes, the wedge can be quite bulky and impede the generation of shear waves close to the edge of the weld crown. For this reason, the ultrasound waves arrive to the region to inspect after a single or double bounce at the back wall of the part, respectively known as V-transmission and W-transmission [32]. This work considers the case of the W-transmission, since this is the case where the ultrasonic waves travel more distance. Pettigrew et al. demonstrated that it is acceptable and convenient to interpret the data obtained from reflected ultrasonic waves in mirrored schematic representation [33]. Therefore, for the preparation of this inspection mode and for the interpretation of its results, it is common practice to illustrate the propagation of the shear ultrasonic rays in a schematic representation obtained through mirroring the geometry (in Figure 7) twice, with respect to the bottom plane, and appending the resulting mirrored copies to the bottom of the original geometry. The result of this operation is shown in Figure 8.

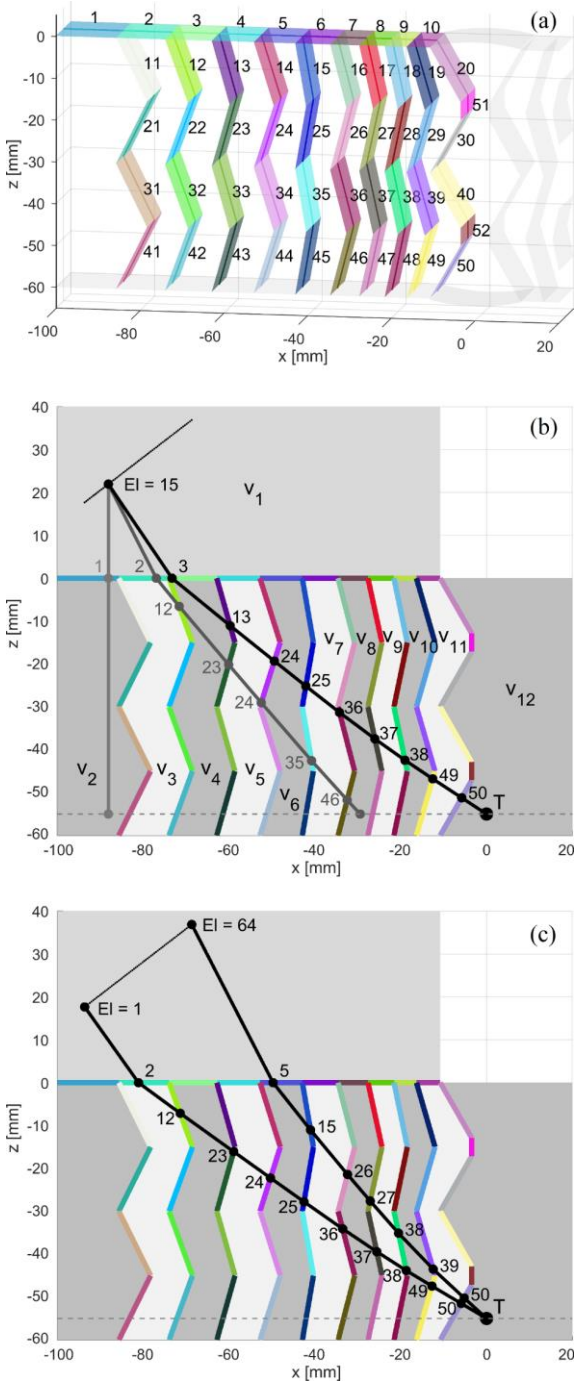

Figure 8 – (a) ~~Tri-dimensional~~ Three dimensional view of all analytical interfaces in the final model, (b) interfaces intersected by the rays produced with the bisection method for the 15th element of the PA probe and (c) interfaces intersected by the final rays for the 1st and the 64th element of the probe.

The final model contains 52 interface surfaces. The horizontal superficial interfaces at the top of the welded plate, analytically defined by Equation 41, are indexed with the numbers from 1 to 10. The remaining surfaces with indices from 11 to 20 and the root face indexed with the number 51, respectively defined by Equation 42 and 43, are mirrored twice with respect to the x-y plane and translated vertically, producing the analytical surfaces indexed with the numbers from 21 to 50 and 52. Figure 8a shows a ~~tri-dimensional~~ three dimensional view of the final model, where each analytical surface is plotted with its given index and with a different colour, to ease the individuation of all surfaces. Figure 8b shows a side view of the representation and illustrates how the surfaces intersected by the ultrasonic rays, computed through the iterations of the generalised bisection method, can be

different for each ray. The same applies to the final rays (originating from the convergence of the method), as shown in Figure 8c. The indices of the intersected surfaces are reported next to the relative intersection points. This work assumes the use of a 64 element 0.5mm pitch 5MHz PA probe, mounted on a wedge with a nominal incidence angle of 37.6 degrees. The centre of the first element of the array is located at $x = -93.65\text{mm}$ and $z = 17.68\text{mm}$. The target (T) is located at $x = 0.00\text{mm}$ and $z = -55.00\text{mm}$. It is assumed that the in-process inspection of the weld is executed by bringing the wedge into contact with the surface of the hot plate only for few seconds, the time required to trigger the elements of the probe and receive the returning ultrasonic echoes. For this assumption, the heat transfer between the wedge material and the plate is neglected. The wedge temperature is assumed to stay constant and the temperatures of the plate regions to be unaffected by the contact with the wedge. Table 1 gives the coordinates of all key points shown in Figure 7b~~c~~ and the shear velocities indicated in Figure 8b. Whereas the shear velocity in the wedge is indicated with v_1, the shear velocities in the welded plate regions are specified with v_2, v_3, …, and v_{12}.

Table 1 – Coordinates of key points of the welded sample model.

Key point coordinates [mm]						**Shear velocity [m/s]**	
Point	**x**	**z**	**Point**	**x**	**z**	v_1	2340
P_0	-150.0	0.00	P_{11}	-78.27	-15.00	v_2	3281
P_1	-85.68	0.00	P_{12}	-68.53	-15.00	v_3	3258
P_2	-73.98	0.00	P_{13}	-58.62	-15.00	v_4	3235
P_3	-62.85	0.00	P_{14}	-48.07	-15.00	v_5	3213
P_4	-52.79	0.00	P_{15}	-40.34	-15.00	v_6	3180
P_5	-42.92	0.00	P_{16}	-30.73	-15.00	v_7	3138
P_6	-34.59	0.00	P_{17}	-24.37	-15.00	v_8	3084
P_7	-27.63	0.00	P_{18}	-18.47	-15.00	v_9	3018
P_8	-21.57	0.00	P_{19}	-12.01	-15.00	v_{10}	2940
P_9	-16.33	0.00	P_{20}	-3.46	-15.00	v_{11}	2848
P_{10}	-10.80	0.00	P_{21}	-3.46	-12.88	v_{12}	2768

Due to the limited size of the horizontal interfaces and the high tilt of the volumetric interfaces, each ultrasonic ray intersects a different subset of interface surfaces, as indicated above and shown in Figure 8b and Figure 8c. Therefore, the introduced generalization of the bisection method, described in Section 5, has been refined to cope with this additional challenge. For every refraction, the analytic equation of the line for the last intersection point, whose direction is given by the unitary refraction vector ($\vec{r}$), is intersected in turn with all the analytic functions of the interfaces. This operation gives one intersection point for each interface surface. The interface that produces the closest point to the last intersection point is selected as the correct intersection surface and the point is returned as the location where a new refraction takes place. This continues until the horizontal plane for the target (T) is reached.

The generalized bisection method was first used to compute the ray tracing for three easy cases, assuming a constant temperature of 140°C, 460°C and 780°C (see Figure 9a-c). Respectively, shear velocities of 3281, 3180 and 2940 m/s were used for the whole welded plate, for the three cases. ~~The iterations of the bisection method were stopped at errors smaller than 0.01mm.~~ Obtaining a distance from target smaller than 0.01mm has been used as stopping criterion in our work, to stop the iterations of the bisection method. Note, the stopping criterion can be different, depending on the application. In practical applications of the method, a meaningful approach would be to stop iterating when the change in transit time is smaller than a defined fraction of a wavelength. Then, the resulting incidence vectors for the PA sources were propagated through the interface surfaces of the

reference model with multiple temperature (see Figure 9d-f). This demonstrates that, when assuming constant temperature for the welded plate, accurate ultrasonic focusing can be seriously compromised in in-process inspection scenarios. Indicating with O_m the average minimum distance between the target point and the ultrasonic rays, the propagation of the incidence vectors produces, for the three cases, average distances equal to 3.00, 5.93 and 13.71mm.

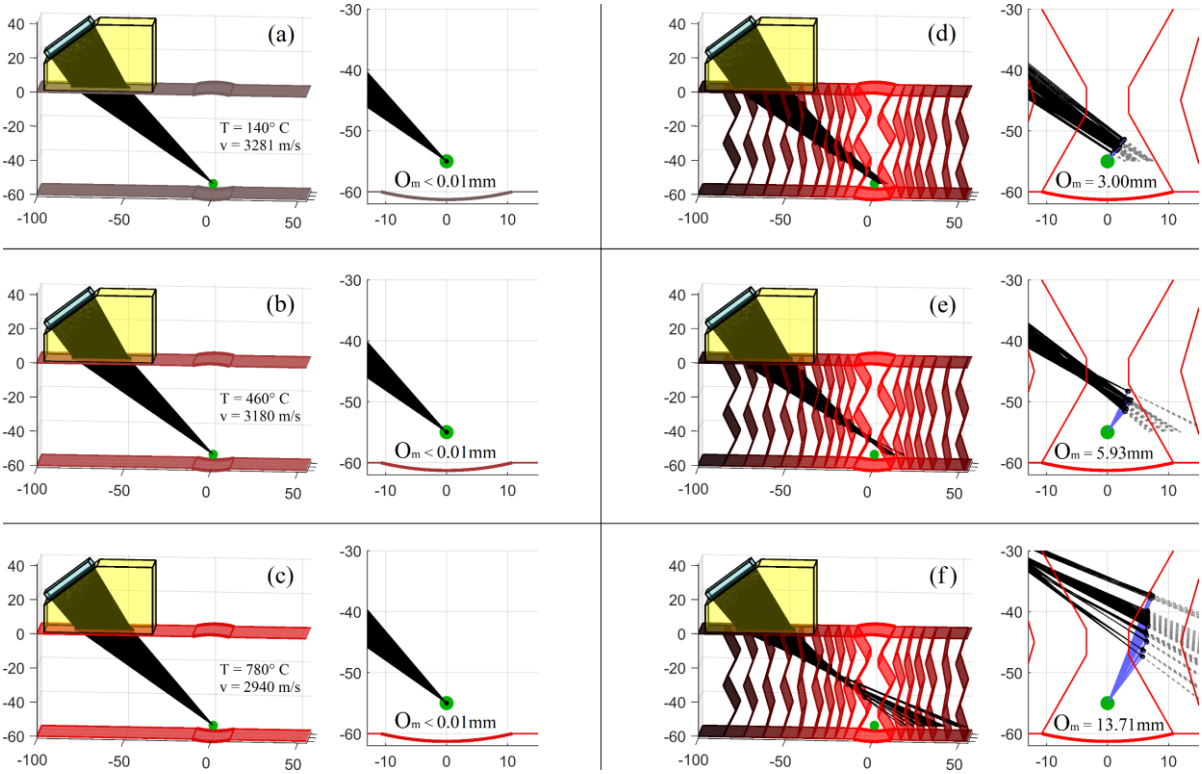

Figure 9 – Ray tracing from all PA sources to the target point assuming constant temperatures of 140°C (a), 460°C (b) and 780°C (c) for the welded plate. Propagation of the resulting incidence vectors to the reference model with multiple regions separated by interface surfaces (d, e and f).

The introduced bisection method was applied to the reference model, considering all its 52 interface surfaces, to find the optimum incidence angle for all the ultrasonic rays originating from the phased array elements, in order to focus the ultrasonic waves at the target. As for the constant temperature cases, here also, the iterations of the bisection method were stopped at errors smaller than 0.01mm. Figure 10 gives evidence of the result. The method enabled the accurate computation of the PA rays to achieve optimum focusing at the target. The generalised bisection method was implemented in Matlab 2020b and tested in a computer with an Intel® i7-6820HQ CPU (2.70GHz, 4 Cores) and 32Gb of Random-Access Memory. Table 2 reports quantitative performance results for the execution of the generalized bisection method in the constant temperature models and in the variable temperature model, in terms of average number of iterations, average duration of each iteration, average convergence time per each ray and total elapsed~~, time at convergence,~~ Table 3 reports the minimum and maximum travel times and distances for each test case and the relative errors, in terms of resulting mean and maximum ~~and mean~~ distances from target and shift in ultrasonic ray travel time. As expected the iterative method converges in less than ~~50sec~~ 4sec when a constant temperature is assumed for the whole welded plate, since only one interface is present in this case (the interface between the wedge and the plate). However, the assumption of constant temperature causes distances as large as 19.3mm between the ultrasonic rays and the target point and shifts in travel time as big as 17.5μs. The maximum distance is kept below 0.01mm, when the bisection method

is applied to the full reference model with 11 temperature zones and 52 interface surfaces. In this case, the computation converges in ~~21~~ 15 minutes and ~~10.5~~19 seconds. In order to investigate the relationship between the computation time and the number of interfaces, ~~an~~ additional tests were~~as~~ carried out interpolating~~halving the number of~~ the discrete temperature zones in the model, ~~resulting~~in order to generate five additional test models ~~in~~ with 2, 4, 6, 8 and 10 zones and 7, 17, 27, 37 and 47 ~~27~~ interfaces respectively. ~~The temperature zones of the full model were merged two by two, removing the separation surfaces in the middle of each couple and assigning average propagation speeds to the resulting temperature zones. In this case, the method converged in slightly less than 8 minutes. This seems to suggest that the~~ The resulting elapsed times in Table 2 show a quadratic dependence between the computation time of the current method and the number of surfaces in the model ~~could be described by a linear or a sub-quadratic law~~.

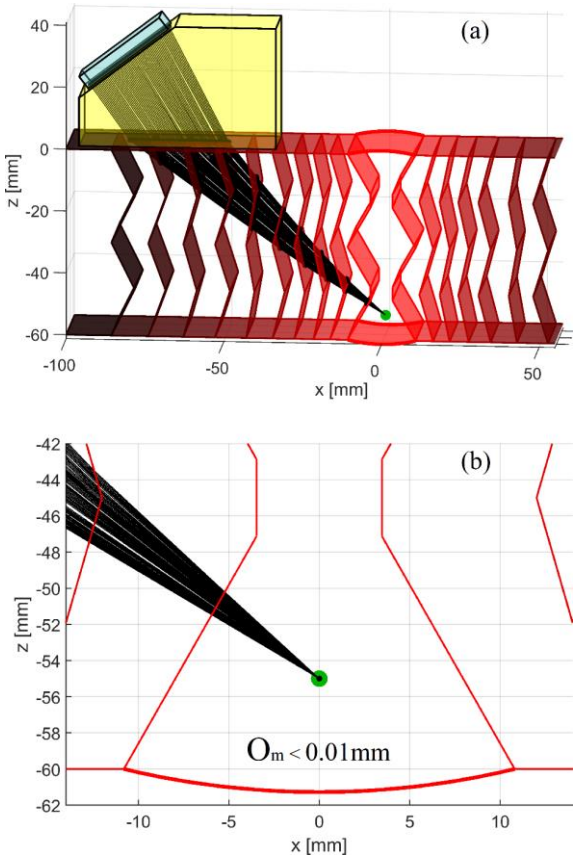

Figure 10 – Ray tracing from all phased array sources to the target point in the reference sample (a) and close up image of the area around the target (b).

Table 2 – ~~Quantitative performance results~~Computation times.

Temperature of model used for computation	**Num. of interfaces**	**Num. ~~elem.~~rays**	**Average num. of iterations**	**Average duration of each iteration [ms]**	**Average convergence time per ray [s]**	**Total ~~E~~elapsed time ~~at convergence~~**
Constant (140˚C)	1	64	13.20	3.98	0.0527	~~41.9~~ 3.3753 s~~ec~~
Constant (460˚C)	1	64	13.51	3.87	0.0523	~~41.5~~ 3.3451 s~~ec~~
Constant (780˚C)	1	64	13.45	3.91	0.0526	~~41.8~~ 3.3645 s~~ec~~
2 zones	7	64	13.64	21.86	0.2982	19.0830 s
4 zones	17	64	13.83	96.14	1.3295	1’ 25.0879 s
6 zones	27	64	13.98	230.65	3.2255	3’ 26.4329 s
8 zones	37	64	15.67	449.48	7.0443	7’ 30.8321 s
10 zones	47	64	14.91	759.96	11.3281	12’ 5.0014 s
Ref. model (11 zones)	52	64	14.95	960.36	14.3603	15’ 19.0600 s

Table 3 – Distances and transit times (absolute and relative).

	Absolute travel distance and time				Evaluation in reference model with 11 zones			
Temperature of model used for computation	**Min transit distance [mm]**	**Max transit distance [mm]**	**Min transit time [µs]**	**Max transit time [µs]**	**Mean distance from target (O_m) [mm]**	**Max distance from target [mm]**	**Mean shift in transit time [µs]**	**Max shift in transit time [µs]**
Constant (140˚C)	115.4547	119.5808	39.1287	40.3255	2.9995	4.5881	1.5774	2.4261
Constant (460˚C)	115.3408	119.4464	40.0723	41.0339	5.9310	7.5542	3.4099	5.5051
Constant (780˚C)	115.0820	119.1156	42.4144	42.8997	13.7115	19.2990	9.3275	17.4573
2 zones	114.9971	118.9979	43.4097	43.7610	16.8022	25.4787	11.8421	25.5825
4 zones	115.4540	119.7607	41.5273	42.9150	3.9199	5.9205	1.8740	2.8408
6 zones	115.6486	119.8180	41.1850	42.6217	1.4377	2.1348	0.6899	1.1720
8 zones	115.6218	119.7808	41.0746	42.5057	1.1135	2.6651	0.5349	1.2874
10 zones	115.8426	119.7384	41.0016	42.4173	0.7981	2.1470	0.3735	0.7879
Ref. model (11 zones)	115.7414	119.7349	40.9628	42.3805	0.0028	0.0062	null	null

Although the method has not been optimized for speed so far and more sophisticated implementations can minimize the execution time in the future, the current result is already a great advantage if compared to the time required by Finite Element models, which is in the order of few days, to perform ray tracing for the scenario examined in this work. Nevertheless, the proposed approach can be used to pre-calculate a number of focal laws for the geometry, but with differing temperature profiles. During the inspection, temperature sensors can be used to select the most appropriate match for the thermal profile.

7. CONCLUSIONS

Ultrasonic testing is still a hot research topic. The desire to apply ultrasonic testing to geometrically complex structures, and to anisotropic, inhomogeneous materials, together with the advent of more powerful electronics and software, is constantly pushing the applicability of ultrasonic ways to their limits. General ray tracing models are currently required, to support the development of new imaging techniques, such as Full Matrix Capture and Total Focusing Method, and the execution of challenging inspections. One existing solution is to implement the Fast-Marching Method (FMM) combined with Fermat's principle and Dijkstra's algorithm. This paper introduced a generalized iterative method for the computation of ultrasonic ray paths, when ultrasonic source and target are separated by multiple complex material interfaces in the ~~bi~~ two dimensional and ~~tri dimensional~~ three dimensional domains. The method was implemented in Matlab 2020b. Starting from a review of the well-known bisection method, this work extends the applicability of the method to cases with increasing complexity and to the ~~tri dimensional~~ three dimensional domain. An application example, in the field of in-process weld inspection, was presented. The generalised bisection method enabled the computation of optimum incidence angles to achieve accurate ultrasonic focusing, through a 64-element phased array probe mounted on a wedge and a model with 52 interface surfaces. The maximum distance between the ultrasonic rays and the target is kept below 0.01mm and the computation converged in 21 minutes. Although the implementation of the method was not optimized for speed, the current result is already a great advantage if compared to the time required by Finite Element models. Future work will focus on generating more sophisticated implementations of the method, capable of minimizing the execution time without compromising the accuracy.

ACKNOWLEDGEMENTS

This work has received funding from the European Union's Horizon 2020 research and innovation programme under the Marie Sklodowska-Curie grant agreement No 835846. Furthermore, the authors would like to thank Dr Zhen Qiu (University of Strathclyde) for providing the temperature field data of the butt-welded plates, which derived from work done for the project EP/R004889/1 - Delivering Enhanced Through-Life Nuclear Asset Management (funded by the ANRC 12-1 call on Advanced Ultrasonic Inspection and Monitoring for Challenging Industrial Welding Applications).

REFERENCES

[1] L. Mordfin, *Handbook of reference data for nondestructive testing*. ASTM, 2002.
[2] B. W. Drinkwater and P. D. Wilcox, "Ultrasonic arrays for non-destructive evaluation: A review," *NDT & e International,* vol. 39, no. 7, pp. 525-541, 2006.
[3] A. J. Hunter, B. W. Drinkwater, and P. D. Wilcox, "Autofocusing ultrasonic imagery for non-destructive testing and evaluation of specimens with complicated geometries," *Ndt & E International,* vol. 43, no. 2, pp. 78-85, 2010.
[4] S. Mahaut, O. Roy, C. Beroni, and B. Rotter, "Development of phased array techniques to improve characterization of defect located in a component of complex geometry," *Ultrasonics,* vol. 40, no. 1-8, pp. 165-169, 2002.
[5] J. Zhang, B. W. Drinkwater, P. D. Wilcox, and A. J. Hunter, "Defect detection using ultrasonic arrays: The multi-mode total focusing method," *NDT & e International,* vol. 43, no. 2, pp. 123-133, 2010.
[6] B. Drinkwater and A. Bowler, "Ultrasonic array inspection of the Clifton Suspension Bridge chain-links," *Insight-Non-Destructive Testing and Condition Monitoring,* vol. 51, no. 9, pp. 491-498, 2009.
[7] J. Russell, R. Long, D. Duxbury, and P. Cawley, "Development and implementation of a membrane-coupled conformable array transducer for use in the nuclear industry," *Insight-Non-Destructive Testing and Condition Monitoring,* vol. 54, no. 7, pp. 386-393, 2012.
[8] C. Mineo, S. Pierce, B. Wright, I. Cooper, and P. Nicholson, "PAUT inspection of complex-shaped composite materials through six DOFs robotic manipulators," *Insight-Non-Destructive Testing and Condition Monitoring,* vol. 57, no. 3, pp. 161-166, 2015.
[9] J. Zhang, B. W. Drinkwater, and P. D. Wilcox, "Efficient immersion imaging of components with nonplanar surfaces," *IEEE transactions on ultrasonics, ferroelectrics, and frequency control,* vol. 61, no. 8, pp. 1284-1295, 2014.
[10] M. Sutcliffe, M. Weston, P. Charlton, K. Donne, B. Wright, and I. Cooper, "Full matrix capture with time-efficient auto-focusing of unknown geometry through dual-layered media," *Insight-Non-Destructive Testing and Condition Monitoring,* vol. 55, no. 6, pp. 297-301, 2013.
[11] J. Ye *et al.*, "Development of an ultrasonic ray model for phased array ultrasonic testing in austenitic weldments," in *17th World Conference on Non-Destructive Testing, Shanghai*, 2008, pp. 25-28.
[12] O. Nowers, D. J. Duxbury, J. Zhang, and B. W. Drinkwater, "Novel ray-tracing algorithms in NDE: Application of Dijkstra and A⋆ algorithms to the inspection of an anisotropic weld," *NDT & E International,* vol. 61, pp. 58-66, 2014.
[13] K. M. M. Tant, E. Galetti, A. Mulholland, A. Curtis, and A. Gachagan, "Effective grain orientation mapping of complex and locally anisotropic media for improved imaging in ultrasonic non-destructive testing," *Inverse Problems in Science and Engineering,* pp. 1-25, 2020.
[14] R. L. Burden and J. D. Faires, "2.1 The bisection algorithm," *Numerical analysis,* 1985.
[15] A. Rontó and M. Rontó, "Periodic successive approximations and interval halving," *Miskolc Mathematical Notes,* vol. 13, no. 2, pp. 459-482, 2012.
[16] A. Boultif and D. Louër, "Indexing of powder diffraction patterns for low-symmetry lattices by the successive dichotomy method," *Journal of Applied Crystallography,* vol. 24, no. 6, pp. 987-993, 1991.
[17] A. S. Glassner, "An Introduction to Ray Tracing Morgan Kaufmann," ed: London, 1989.
[18] M. Born and E. Wolf, "1970Principles of optics," *and,* vol. 11, p. 1.
[19] C. Macleod *et al.*, "Dry-coupled automated inspection for wire+ arc additive manufacture," *Review of Progress in Quantitative Nondestructive Evaluation,* 2019.
[20] C. Mineo, S. G. Pierce, P. I. Nicholson, and I. Cooper, "Robotic path planning for non-destructive testing–A custom MATLAB toolbox approach," *Robotics and Computer-Integrated Manufacturing,* vol. 37, pp. 1-12, 2016.
[21] C. Mineo, "Automated NDT inspection for large and complex geometries of composite materials," University of Strathclyde, 2015.
[22] Y. Javadi *et al.*, "Ultrasonic phased array inspection of a Wire+ Arc Additive Manufactured (WAAM) sample with intentionally embedded defects," *Additive Manufacturing,* vol. 29, p. 100806, 2019.
[23] Y. Javadi *et al.*, "Continuous monitoring of an intentionally-manufactured crack using an automated welding and in-process inspection system," *Materials & Design,* p. 108655, 2020.
[24] Y. Javadi *et al.*, "Investigating the effect of residual stress on hydrogen cracking in multi-pass robotic welding through process compatible non-destructive testing," *Journal of Manufacturing Processes,* 2020.
[25] Y. Javadi *et al.*, "In-process calibration of a non-destructive testing system used for in-process inspection of multi-pass welding," *Materials & Design,* p. 108981, 2020.

[26] D. Lines *et al.*, "A flexible robotic cell for in-process inspection of multi-pass welds," *Insight-Non-Destructive Testing and Condition Monitoring*, vol. 62, no. 9, pp. 526-532, 2020, doi: 10.1784/insi.2020.62.9.526.
[27] Z. Qiu *et al.*, "Study of Thermal Gradient Effect for In-Process Ultrasonic Inspection of Fusion Welding," presented at the IEEE International Ultrasonics Symposium (IUS), Glasgow (UK), 2019.
[28] *Non-destructive testing of welds. Ultrasonic testing. Techniques, testing levels, and assessment*, BS EN ISO 17640:2018.
[29] *Non-destructive testing of welds. Ultrasonic testing. Use of automated phased array technology*, BS EN ISO 13588:2019.
[30] *Non-destructive testing of welds. Phased array ultrasonic testing (PAUT). Acceptance levels*, BS EN ISO 19285:2017.
[31] U. Ewert *et al.*, "Performance Control: Nondestructive Testing and Reliability Evaluation," in *Springer Handbook of Metrology and Testing*, H. Czichos, T. Saito, and L. Smith Eds. Berlin, Heidelberg: Springer Berlin Heidelberg, 2011, pp. 887-972.
[32] I. Burhan, G. Mutaiyah, D. I. Hashim, T. M. Loganathan, and M. T. H. Sultan, "A Guideline of Ultrasonic Inspection on Butt Welded Plates," in *IOP Conference Series: Materials Science and Engineering*, 2019, vol. 554, no. 1: IOP Publishing, p. 012002.
[33] I. G. Pettigrew, D. I. A. Lines, K. J. Kirk, and S. Cochran, "Investigation of crack sizing using ultrasonic phased arrays with signal processing techniques," *Insight-Non-Destructive Testing and Condition Monitoring*, vol. 48, no. 2, 2006.

APPENDICES

Appendix A

System with the equation of the line for the source P_{i-1}, whose direction is given by the unitary vector ($\vec{r}_i$), and the equation relative to the i^{th} interface, $z = f_i(x, y)$. The solution of this system leads to the coordinates $\left(P_i^x, P_i^y\right)$ of the incidence points, from the 2nd to the $(k-1)^{\text{th}}$ incidence points.

if $\left(r_i^x \neq 0, r_i^y \neq 0, r_i^z \neq 0\right)$

$$\begin{cases} line\ for\ P_{i-1}: & \begin{cases} \dfrac{x - P_{i-1}^x}{r_i^x} = \dfrac{y - P_{i-1}^y}{r_i^y} \\ \dfrac{y - P_{i-1}^y}{r_i^y} = \dfrac{z - P_{i-1}^z}{r_i^z} \end{cases} \\ i^{th}\ interface: & z = f_i(x, y) \end{cases}$$

elseif $\left(r_i^x = 0, r_i^y \neq 0, r_i^z \neq 0\right)$

$$\begin{cases} line\ for\ P_{i-1}: & \begin{cases} x = P_{i-1}^x \\ \dfrac{y - P_{i-1}^y}{r_i^y} = \dfrac{z - P_{i-1}^z}{r_i^z} \end{cases} \\ i^{th}\ interface: & z = f_i(x, y) \end{cases}$$

elseif $\left(r_i^x \neq 0, r_i^y = 0, r_i^z \neq 0\right)$

$$\begin{cases} line\ for\ P_{i-1}: & \begin{cases} y = P_{i-1}^y \\ \dfrac{x - P_{i-1}^x}{r_i^x} = \dfrac{z - P_{i-1}^z}{r_i^y} \end{cases} \\ i^{th}\ interface: & z = f_i(x, y) \end{cases}$$

elseif $\left(r_i^x \neq 0, r_i^y \neq 0, r_i^z = 0\right)$

$$\begin{cases} line\ for\ P_{i-1}: & \begin{cases} z = P_{i-1}^z \\ \dfrac{x - P_{i-1}^x}{r_i^x} = \dfrac{y - P_{i-1}^y}{r_i^y} \end{cases} \\ i^{th}\ interface: & z = f_i(x, y) \end{cases}$$

elseif $\left(r_i^x = 0, r_i^y = 0, r_i^z \neq 0\right)$

$$\begin{cases} line\ for\ P_{i-1}: & \begin{cases} x = P_{i-1}^x \\ y = P_{i-1}^y \end{cases} \\ i^{th}\ interface: & z = f_i(x, y) \end{cases}$$

elseif $\left(r_i^x = 0, r_i^y \neq 0, r_i^z = 0\right)$

$$\begin{cases} line\ for\ P_{i-1}: & \begin{cases} x = P_{i-1}^x \\ z = P_{i-1}^z \end{cases} \\ i^{th}\ interface: & z = f_i(x,y) \end{cases}$$

elseif $\left(r_i^x \neq 0, r_i^y = 0, r_i^z = 0\right)$

$$\begin{cases} line\ for\ P_{i-1}: & \begin{cases} y = P_{i-1}^y \\ z = P_{i-1}^z \end{cases} \\ i^{th}\ interface: & z = f_i(x,y) \end{cases}$$

end

Appendix B

System containing the equation of the line for the point P_{k-1} and the horizontal plane for T ($z = T^z$). The solution of this system leads to the coordinates $\left(T_0^x, T_0^y, T_0^z\right)$ of the resulting target point, related to the initial guess angle θ_1 (given as input).

if $\left(r_i^x \neq 0, r_i^y \neq 0, r_i^z \neq 0\right)$

$$\begin{cases} line\ for\ P_{i-1}: & \begin{cases} \dfrac{x - P_{i-1}^x}{r_i^x} = \dfrac{y - P_{i-1}^y}{r_i^y} \\ \dfrac{y - P_{i-1}^y}{r_i^y} = \dfrac{z - P_{i-1}^z}{r_i^z} \end{cases} \\ horiz.plane\ for\ T: & z = T^z \end{cases}$$

elseif $\left(r_i^x = 0, r_i^y \neq 0, r_i^z \neq 0\right)$

$$\begin{cases} line\ for\ P_{i-1}: & \begin{cases} x = P_{i-1}^x \\ \dfrac{y - P_{i-1}^y}{r_i^y} = \dfrac{z - P_{i-1}^z}{r_i^z} \end{cases} \\ horiz.plane\ for\ T: & z = T^z \end{cases}$$

elseif $\left(r_i^x \neq 0, r_i^y = 0, r_i^z \neq 0\right)$

$$\begin{cases} line\ for\ P_{i-1}: & \begin{cases} y = P_{i-1}^y \\ \dfrac{x - P_{i-1}^x}{r_i^x} = \dfrac{z - P_{i-1}^z}{r_i^y} \end{cases} \\ horiz.plane\ for\ T: & z = T^z \end{cases}$$

elseif $\left(r_i^x \neq 0, r_i^y \neq 0, r_i^z = 0\right)$

$$\begin{cases} line\ for\ P_{i-1}: & \begin{cases} z = P_{i-1}^z \\ \dfrac{x - P_{i-1}^x}{r_i^x} = \dfrac{y - P_{i-1}^y}{r_i^y} \end{cases} \\ horiz.plane\ for\ T: & z = T^z \end{cases}$$

elseif $\left(r_i^x = 0, r_i^y = 0, r_i^z \neq 0\right)$

$$\begin{cases} line\ for\ P_{i-1}: & \begin{cases} x = P_{i-1}^x \\ y = P_{i-1}^y \end{cases} \\ horiz.plane\ for\ T: & z = T^z \end{cases}$$

elseif $\left(r_i^x = 0, r_i^y \neq 0, r_i^z = 0\right)$

$$\begin{cases} line\ for\ P_{i-1}: & \begin{cases} x = P_{i-1}^x \\ z = P_{i-1}^z \end{cases} \\ horiz.plane\ for\ T: & z = T^z \end{cases}$$

elseif $\left(r_i^x \neq 0, r_i^y = 0, r_i^z = 0\right)$

$$\begin{cases} line\ for\ P_{i-1}: & \begin{cases} y = P_{i-1}^y \\ z = P_{i-1}^z \end{cases} \\ horiz.plane\ for\ T: & z = T^z \end{cases}$$

end

AUTHOR DECLARATION

Conflict of interest

We wish to confirm that there are no known conflicts of interest associated with this publication and there has been no significant financial support for this work that could have influenced its outcome. We confirm that the manuscript has been read and approved by all named authors and that there are no other persons who satisfied the criteria for authorship but are not listed. We further confirm that the order of authors listed in the manuscript has been approved by all of us. We confirm that we have given due consideration to the protection of intellectual property associated with this work and that there are no impediments to publication, including the timing of publication, with respect to intellectual property. In so doing we confirm that we have followed the regulations of our institutions concerning intellectual property.

We understand that the Corresponding Author is the sole contact for the Editorial process (including Editorial Manager and direct communications with the office). He is responsible for communicating with the other authors about progress, submissions of revisions and final approval of proofs. We confirm that we have provided a current, correct email address which is accessible by the Corresponding Author.

This document is signed by the corresponding author on behalf of all authors.

Carmelo Mineo, 21st October 2020